



HAL
open science

Echofacies interpretation of Pleistocene to Holocene contourites on the Demerara plateau and abyssal plain

Cédric Tallobre, Lies Loncke, Laurence Droz, Tania Marsset, Mirjam Uusõue, Walter Roest, Anne-Sophie Fanget, Maria-Angela Bassetti, Pierre Giresse, Germain Bayon

► To cite this version:

Cédric Tallobre, Lies Loncke, Laurence Droz, Tania Marsset, Mirjam Uusõue, et al.. Echofacies interpretation of Pleistocene to Holocene contourites on the Demerara plateau and abyssal plain. Interpretation-A Journal of Subsurface Characterization, 2021, 9 (2), pp.SB49-SB65. 10.1190/INT-2020-0159.1 . hal-04203342

HAL Id: hal-04203342

<https://hal.science/hal-04203342v1>

Submitted on 19 Nov 2024

HAL is a multi-disciplinary open access archive for the deposit and dissemination of scientific research documents, whether they are published or not. The documents may come from teaching and research institutions in France or abroad, or from public or private research centers.

L'archive ouverte pluridisciplinaire **HAL**, est destinée au dépôt et à la diffusion de documents scientifiques de niveau recherche, publiés ou non, émanant des établissements d'enseignement et de recherche français ou étrangers, des laboratoires publics ou privés.

Echofacies interpretation of Pleistocene to Holocene contourites on the Demerara plateau and abyssal plain

Tallobre Cédric ¹, Loncke Lies ¹, Droz Laurence ², Marsset Tania ³, Uusõue Mirjam ⁴, Roest Walter ³,
Fanget Anne-Sophie ¹, Bassetti Maria-Angela ¹, Giresse Pierre ¹, Bayon Germain ³

¹ Université de Perpignan Via Domitia, Centre de Formation et de Recherche sur les Environnements Méditerranéens (CEFREM), UMR 5110, Perpignan, France..

² Université de Bretagne Occidentale (UBO)/UMR 6538 du CNRS Domaines Océaniques, Plouzané, France..

³ IFREMER, Unité de Recherche Géosciences Marines, Plouzané, France..

⁴ Tartu Observatory, Observatooriumi 1, Tõravere, 61602 Tartumaa, Estonia..

Email addresses : cedrictallobre@rocketmail.com ; lies.loncke@univ-perp.fr ; laurence.droz@univ-brest.fr ; tania.marset@ifremer.fr ; mirjam.uusoue@ut.ee ; walter.roest@ifremer.fr ; annesophie.fanget@gmail.com ; maria-angela.bassetti@univ-perp.fr ; pierre.giresse@univ-perp.fr; germain.bayon@ifremer.fr

Abstract :

Off French Guiana and Surinam, NADW and AABW oceanic currents contour the Demerara marginal plateau, which promotes the formation of contourites. We have studied these contourites thanks to a new compilation of high-resolution sub-bottom profiles calibrated by sedimentary cores. The echo-facies and isopach maps we constructed highlight a sedimentary distribution parallel to the isobaths. The presence of moats along the slope is confirmed by the observation of parallel, elongated, sedimentary depleted zones and echo-facies strongly affected by diffraction hyperbola and transparent echo-facies. We interpret these features to be related to eroded slopes and Mass Transport Deposits. In contrast, the sedimentary drifts we mapped are characterized by elongated and thick slope-parallel depocentres displaying bedded echo-facies with wave-like bedforms. According to our interpretation, they result from interactions between currents and the seafloor. Seismic wipe-outs frequently affect those drifts, possibly resulting from high water or organic contents.

21 **Introduction**

22 The mapping, identification, and improved understanding of contourites has numerous
23 implications. (1) Contourites, which are formed by bottom currents, in particular those
24 deposited in relation with thermohaline bottom currents, are known to record current intensity

25 variations through time. Thus, they form high interest sedimentary archives for documenting
26 palaeoceanographic variations (Knutz, 2008; Rebesco et al., 2014) and constrain palaeoclimate
27 models. (2) Moreover, Contourite Depositional Systems (CDS) are frequently associated with
28 slope instability as high accumulation rates and significant water content inside the drifts (i.e.,
29 sedimentary depositional structure in contourites) induce low consolidation and overall
30 decrease of shear-stress resistance (Mulder et al., 2003; Hanquiez et al., 2010; Ducassou et al.,
31 2016). In turn, erosion along contouritic channels, caused by the winnowing effect of bottom
32 currents, can decrease cohesion and resisting forces and hence promote geohazards (Ingram et
33 al., 2011). (3) Several publications highlight the interest of contourites in hydrocarbon
34 exploration, as muddy contourites often rich in organic matter can act as potential source rock
35 or seal (Viana, 2008), whereas sandy contourites can form good reservoir containers due to
36 their high porosity and permeability (Enjorlas et al., 1986; Viana, 2008).

37 Since their first description using seafloor photography (Heezen, 1959; Heezen and
38 Johnson, 1963; Heezen and Hollister, 1964), contouritic deposits and processes have been
39 studied in a wide variety of settings and by numerous methods, including geophysical
40 (bathymetry, sub-bottom and seismic profiling), sedimentological (coring, core logging and
41 numerous approaches to characterize the sediment) and oceanographical (mooring records and
42 data). Despite significant progress in the recognition of contourites and their role in margin
43 sedimentary patterns, the diversity of these depositional systems still needs diagnostic
44 geophysical and sedimentary criteria in order to recognize them at different scales and relate
45 them to complex 3D and temporally changing oceanographic processes.

46 Two Contourite Depositional Systems (CDS) have been described offshore French Guiana
47 and Suriname in relation with the Demerara Plateau (Loncke et al., 2009; de Lépinay et al.,
48 2016; Loncke et al., 2016; Tallobre et al., 2016; Tallobre et al., 2019; Fanget et al., 2020), which
49 forms a salient planar bathymetric relief 350 km from the coast (Figure 1). One CDS is related

50 to the southward flowing North Atlantic Deep Water (NADW) and developed on the plateau
51 itself (the “NADW CDS”). This CDS emplaced in the very distal part of the Demerara Plateau
52 and is isolated from continental terrigenous sediment supplies. Therefore, sediments nearly
53 exclusively record the along-slope flow of the NADW bottom current (Tallobre et al., 2016;
54 Tallobre et al., 2019; Fanget et al., 2020). A second CDS is related to the northward flowing
55 Antarctic Bottom Water (AABW), developed at the foot of the plateau, in the Demerara abyssal
56 plain (the “AABW CDS”) (Loncke et al., 2009).

57 The Demerara Plateau has been intensively surveyed in recent years. Four oceanographic
58 cruises, (1) the GUYAPLAC survey (Le Suave and Beuzart, 2003), (2) the IGUANES survey
59 (Loncke, 2013), (3) the DRADEM survey (Basile, 2016) and (4) the MARGATS survey
60 (Graindorge and Klingelhoefer, 2016), enabled the acquisition of an important seismic and sub-
61 bottom profile dataset and of 20 piston cores. The analysis of the GUYAPLAC dataset first
62 provided evidence for the predominance of slope instability in the distal Demerara Plateau
63 (Loncke et al., 2009; Pattier et al., 2013). Subsequently, the high-resolution seismic data
64 acquired during the IGUANES cruise highlighted the role of deep currents on sedimentary
65 patterns and enabled to propose a link between slope instability and contourites at least since
66 the Pliocene (Pattier et al., 2015; Loncke et al., 2016; Tallobre et al., 2016; Fanget et al., 2020).
67 The analysis of sedimentary cores confirmed that recent mid-Pleistocene to Holocene
68 sedimentation is dominated by contourites recording NADW flow intensity variations (Tallobre
69 et al., 2016; Tallobre et al., 2019). Since the very first echo-facies mapping of the Demerara
70 area published by Loncke et al., (2009), the new sub-bottom profiler and core datasets have
71 never been presented in a comprehensive synthesis.

72 The aims of this paper are (1) to present an up-to-date echo-facies and isopach mapping of
73 the Demerara CDS, calibrated by core data, synthesizing this available high-resolution sub-

74 bottom dataset, and (2) to use this high-resolution compilation to complete the existing set of
75 diagnostic criteria for modern/recent CDS on sub-bottom profiles.

76 **Regional setting**

77 **Geological setting**

78 The Demerara Plateau belongs to a class of submarine reliefs referred to as “transform
79 marginal plateaus”, that also includes, for example, the Falklands, Vøring, Sao-Paulo plateaus
80 in the Atlantic (Mercier de Lépinay et al., 2016; Loncke et al., 2020). Those plateaus share
81 common physiographic characteristics forming rectangular or triangular shaped planar reliefs
82 prolonging the continental shelf down to depths varying from 1200 to 3000 m water depth
83 (Figure 2). They all formed through transform-dominated breakups. The Demerara plateau is a
84 Jurassic volcanic plateau (Loncke et al., 2020) that separated from the Guinea plateau during
85 the Cretaceous Equatorial Atlantic highly oblique opening (Gouyet, 1988; Unternehr et al.,
86 1988; Basile et al., 2013). Its specific shape forming a protruding submarine relief along the
87 French Guiana-Surinam margin seems to promote contouritic processes (Tallobre et al., 2016;
88 Loncke et al., 2020).

89 In the case of the Demerara marginal plateau, sedimentation seems to have been weakly
90 influenced by deep currents until the Middle Miocene (Fanget et al., 2020). At the Mid-
91 Miocene/Early Pliocene, a major mass-wasting event eroded the Demerara Plateau down to
92 Palaeocene strata. This event is probably related to major changes in oceanic circulation
93 throughout the Atlantic that led to the establishment of the modern thermohaline circulation
94 and strengthening of the Atlantic Meridional Oceanic Circulation (Niemi et al., 2000; Pfuhl and
95 McCave, 2005; Hernández-Molina et al., 2009; Herold et al., 2012; Uenzelmann-Neben et al.,
96 2017). This major mass-wasting event resulted in the deposition of a thick mass-transport
97 deposit (MTD) in the outer Demerara Plateau called “Lower Miocene/Early Pliocene” Mass-
98 Transport Deposit, figure 3F) (Tallobre et al., 2016; Fanget et al., 2020). The main headscarp

99 of this slope failure, still visible in the present-day bathymetry, guides the North Atlantic Deep
100 Water (NADW) and it is thought to promote the formation of Middle Pliocene to Holocene
101 NADW CDS, which is well expressed on high-resolution seismic data (Fanget et al., 2020).
102 The drifts form along-slope elongated depocentres with a maximum thickness of 450 m.

103 The Pleistocene to Holocene NADW CDS has been examined using high-resolution
104 multibeam bathymetry and acoustic imagery as well as sub-bottom profiles (Tallobre et al.,
105 2016). This analysis highlighted sediment distribution patterns typical of contouritic processes
106 with (1) erosion along the contourite moat (contourite channels) that follows the main Lower
107 Miocene/Early Pliocene slope failure headscarp, and (2) deposition of an elongated drift and
108 several infill drifts further downslope. Within the elongated drift, longitudinal sedimentary
109 features parallel to the NADW flow are interpreted as being formed by bottom currents
110 interacting with irregularities at the top of the MTDs (“ripple crests”, Figure 3). A mooring
111 deployed over 8 months along the drift evidenced a dominantly SE-oriented current flow with
112 a 32.5 cm/s maximum velocity (Tallobre et al., 2016). Numerous elongated scours with comet
113 tails extending toward the South-East, also called comet marks (Figure 3, details B and D),
114 record the NADW flow around the Demerara seafloor (Loncke et al., 2016; Tallobre et al.,
115 2016). Geophysical data attest the existence of sedimentary features (erosional and deposit
116 structures) that demonstrate the strong influence of the bottom current on the seafloor.
117 Moreover, facies of the moat and drift of this modern CDS are represented by muddy sequences
118 with normal and inversely graded trends (Tallobre et al., 2019). In these sequences, glauconite
119 formation can be correlated with the intensity of bottom currents (Tallobre et al., 2016). When
120 the current intensity increases, the winnowing effect on the seafloor generates erosional features
121 in the moat, promoting the accumulation of coarse sediment on the drift and the formation of
122 glauconite in the sediments. In particular, the analysis of sedimentary sequences suggests that

123 the NADW bottom current intensified during glacial stages and decreased during interglacials
124 (Tallobre et al., 2019).

125 **Physiography and Oceanography**

126 The Demerara TMP is 160 km wide and 350 km long, with water depths ranging from 200
127 to 3800 m and forms a seaward promontory extending the continental shelf (Figure 2A). The
128 northern portion of the plateau ends with a steep slope (average slope of 15°) inherited from the
129 Cretaceous transform-dominated opening of the Equatorial Atlantic. The eastern and western
130 edges of the plateau display gentler dipping slopes (around 4°) (Pattier et al., 2013). The
131 Demerara marginal plateau has been divided into four domains (Basile et al., 2013; Pattier et
132 al., 2013; Mercier de Lépinay, 2016):

- 133 - The upper marginal plateau, located between 1200 m and 1400-1500 m water depth, is
134 characterized by a vast surface with a low dip of around 1° (Figure 2B).
- 135 - The intermediate marginal plateau, between 1500 m and 2500-3000 m water depth, is
136 characterized by an average dip of 3°. It is separated from the upper plateau by a
137 headscarp slope failure (Figure 2) around 1400-1500 m, which is the proximal position
138 of numerous MTDs previously described (Loncke et al., 2009; Pattier et al., 2013). The
139 width of the intermediate marginal plateau is highly variable: 50-70 km wide in the
140 eastern part, 25-50 km wide in the northwestern part and extremely reduced or absent in
141 the central area (between 54°W and 53°W).
- 142 - The lower marginal plateau, between 2500-3000 m and 3200-3500 m water depth,
143 shows an average dip of 1° (Figure 2B). Similar to the intermediate plateau, the lower
144 plateau is strongly reduced in its central part, whereas it is more extensive in the eastern
145 area.
- 146 - The lower continental slope, between 3200-3500 m and 4200-4500 m water depth, is
147 characterized by a steep slope of 15° (Figure 2B), with a maximum value of 20° in the

148 northwestern and central areas. It is the boundary between the marginal plateau and the
149 Demerara abyssal plain (Figure 2).

150 In the Atlantic Ocean, the movement of water masses is controlled by the Atlantic
151 Meridional Overturning Circulation system or AMOC (Apel 1988; Talley et al. 2011; Survey
152 2012). It is characterized by the flow of warm and saline surface waters from the tropics to the
153 North Atlantic Ocean and a return southward flow of cold deep waters. Four main water masses
154 compose the AMOC in the tropical area (Reid, 1989; Peterson and Stramma, 1991; Tsuchiya
155 et al., 1994; Stramma and Schott, 1999):

156 - The Tropical Surface Water and the North Tropical Gyre flows northward between
157 0 and 400 m water depth. This water mass interacts with the seafloor on the continental
158 shelf and upper continental slope.

159 - The Antarctic Intermediate Water (AAIW), initiating in the Southern Ocean, flows
160 northward between 400 m and 1200 m water depth (Figure 1 and Figure 2B). The AAIW
161 is in contact with the seafloor on the upper marginal plateau with a measured velocity
162 of 20 cm/s at 400 m and 5 cm/s at 1000 m (Reid, 1989; Peterson and Stramma, 1991;
163 Suga and Talley, 1995).

164 - The North Atlantic Deep Water (NADW), initiating in the North Atlantic, flows
165 southward between 1200 m and 4200 m water depth (Figure 1 and Figure 2B) and is in
166 contact with the seafloor on the intermediate and lower marginal plateaus. Depending
167 on its physical properties (salinity, temperature and velocity) described in the literature,
168 the NADW can be divided into three sub-water masses (Reid, 1989; Molinari et al.,
169 1992; Johns et al., 1993; Tsuchiya et al., 1994; Mauritzen et al., 2002): (1) “the superior”
170 NADW, between 1200 and 2000 m and with a mean velocity of 2.9 cm/s, impacts the
171 upper and intermediate marginal plateaus, including the headscarp slope failure. (2) The
172 “intermediate” NADW, between 2000 to 3500 m, impacts the intermediate marginal

173 plateau with a mean recorded velocity of 6.2 cm/s in this part of the Atlantic Ocean
174 (Reid, 1989; Tsuchiya et al., 1994; Mauritzen et al., 2002). A mean annual velocity of
175 9.5 cm/s (maximum 32.5 cm/s) was measured on the Demerara plateau at 3000 m water
176 depth (Tallobre et al., 2016). (3) The “inferior” (Mauritzen et al., 2002) NADW flows
177 between 3500 and 4200 m with a mean velocity of around 20.3 cm/s and interacts with
178 the seafloor of the lower marginal plateau and the lower continental slope.

179 - The Antarctic Bottom Water (AABW), originating from Antarctica, flows northward
180 below 4500 m water depth (Figure 1 and Figure2B), with measured velocities which can
181 reach 45 cm/s (Reid, 1989; Molinari et al., 1992; Johns et al., 1993; Hogg, 1997) and is
182 mainly in contact with the abyssal plain seafloor.

183 **Data and methods**

184 The multi-beam and sub-bottom profiler datasets compiled and synthesized in this paper
185 were collected during the GUYAPLAC (Le Suave and Beuzart, 2003) IGUANES (Loncke,
186 2013), MARGATS (Graindorge and Klingelhoefer, 2016) and DRADEM (Basile, 2016) cruises
187 (Figure 1B).

188 During the IGUANES cruise, 20 sedimentary cores were collected by Kullenberg piston
189 coring (1.6 t weight; 5 m free fall). The length of the cores varies between 0.57 m and 9.26 m).
190 The cores are located in the eastern part of the Demerara Plateau (Figure 1B): one core is located
191 on the upper marginal plateau, one adjacent to the headscarp slope failure, one on the abyssal
192 plain and the remaining cores on the intermediate marginal plateau on the NADW-related CDS.
193 All cores have been analysed with the Ifremer Multi Sensor Core Logger and were then split
194 and described (Tallobre, 2017). Water contents have been estimated by the weight ratio between
195 the bulk sediment and lyophilized (freeze-dried) sediment. The sedimentation rates are
196 estimated using the chronostratigraphic framework proposed by Tallobre et al. (2019) and the

197 correlation established between the sedimentary cores (using the P-wave velocity obtained with
198 multi-sensor core logging) and the reflectors on sub-bottom profiles (Tallobre, 2017).

199 Multibeam bathymetry and imagery was acquired during the four cruises with a frequency
200 varying from 12 to 24 kHz, depending on acquisition depths. The data were processed with the
201 Caribes software developed by Ifremer and were combined to produce a digital terrain model
202 with a resolution of 50 to 75 m. All data have been integrated into Q-GIS software for analysis
203 and visualization.

204 The sub-bottom profiler (SBP) data were collected during the four cruises, simultaneously
205 with the multi-beam acquisition. The data were acquired using a hull-mounted sub-bottom
206 profiler with single channel source and with frequencies varying from 1.5 to 6.5 kHz, enabling
207 the imaging of the first few hundred meters of sediment below the seafloor. In most cases, sub-
208 bottom profiles were acquired in a synchronized mode with a multibeam ping rate. Depending
209 on the situation and scientific objectives, acquisitions were performed at speeds of 5 to 10 knots.
210 The SBP data were acquired and processed on board (quality control) using Ifremer QC-
211 SUBOP software. The SBP profiles have an average vertical resolution of 20–30 cm and a
212 horizontal resolution of 20 m (500 m water depth) to 60 m (4000 m water depth).

213 The SBP profiles (Figure 1B) were then interpreted using the envelope mode in Kingdom
214 Suite[®] software for main facies interpretation and in the amplitude mode for accurate core
215 calibration. Due to the nature of the data and their resolution, an approach by echo-facies
216 interpretation and mapping was selected with the aim to study the processes which affected the
217 Demerara plateau at a regional scale from the Pleistocene to the Holocene. Ten echo-facies
218 were differentiated on the basis of acoustic penetration, continuity of bottom and sub-bottom
219 reflectors, seafloor topography and internal structures. The extent of each echo-facies was
220 mapped in order to produce an echo-facies map. It was possible to validate some of the defined
221 echo-facies by sediment cores, enabling us to refine and calibrate the interpretation of echo-

222 facies in terms of sediment types and processes (the description and sedimentary logs of all the
223 cores are available in Tallobre, (2017)).

224 In addition, three horizons of reference for correlation between profiles were chosen on the
225 basis of their sharpness, clarity and lateral continuity and have been mapped on the Demerara
226 Plateau. An isopach map in metres was calculated between the seafloor and the deepest of those
227 horizons (see the preliminary isopach map shown in Tallobre et al., (2016) completed and
228 improved in this paper with the inclusion of DRADEM and MARGATS data). To establish this
229 map, two-way travel time values have been converted into depth in metres using the P-wave
230 velocity measured inside sediment cores by a Multi Sensor Core Logger (average 1500 m/s).
231 This deepest horizon shown in yellow in the figures of this paper could not be dated precisely
232 but is thought to be older than 190 kyr, corresponding to Marine Isotopic Stage 7 (Figure 4;
233 chronostratigraphic framework published in Tallobre, (2017) and Tallobre et al., (2019)).

234 **Results and interpretation**

235 **Echo-facies classification**

236

237 Ten echo-facies were differentiated on the basis of acoustic penetration, continuity of
238 bottom and sub-bottom reflectors, seafloor topography and internal structures (Figure 5 and
239 figure 6). Based on a comparison between these echo-facies and the sedimentary facies in cores
240 and previous studies, sedimentary architecture and processes can be tentatively associated with
241 each of the echo-facies (Figure 5):

- 242 - EF-1: Bedded echo-facies consisting of continuous and regular sub-bottom reflectors
243 with high penetration reaching ~80-120 m. This echo-facies is frequently attributed to
244 well-bedded sedimentary units, such as hemipelagic deposits, distal turbidites (Damuth,
245 1980; Lee et al., 2002; Domzig et al., 2009; Loncke et al., 2009; Nakamura et al., 2016;

246 Sanchez-Guillamón et al., 2018) or contourite drifts (Faugères and Stow, 2008). Cores
247 IG-KSF-19 and IG-KSF-02, collected respectively on the upper marginal plateau and in
248 the abyssal plain (Figure 1B and Figure 6), display relatively homogeneous grey muds
249 (silt and clays) with poorly visible bioturbation structures. Their water content reaches
250 49% and 53%, respectively. Erosional surfaces or distinct contact surfaces cannot be
251 detected in the cores, suggesting a uniform hemipelagite or a muddy contourite
252 interpretation (Stow and Faugères, 2008b; Faugères and Mulder, 2011).

253 - EF-2: Wavy bedded echo-facies with continuous, parallel and wavy reflectors.
254 Generally, these echo-types are associated with sediment waves formed by turbiditic or
255 contour currents (Damuth, 1980; Lee et al., 2002; Bahk et al., 2005; Faugères and Stow,
256 2008). On the Demerara Plateau, the orientation of these waves is parallel to the main
257 current direction. Tallobre et al., (2016) interpreted them as longitudinal waves (Figure
258 3C) formed by bottom currents interacting with pre-existing MTD-related seafloor
259 irregularities. Five cores reveal that this echo-facies corresponds to grey-greenish muds
260 and silty-sandy sediments with water contents varying from 44 to 52%. Two cores
261 collected in this echo-type have been particularly studied and detailed in Tallobre et al.,
262 (2019)(IG-KSF-05 and IG-KSF11). These cores show deposits with successive
263 coarsening and fining upward sequences, characteristic of contouritic facies (Stow and
264 Faugères, 2008b; Faugères and Mulder, 2011). They also show glauconite-rich
265 sequences recording the winnowing effect variations of the NADW through time
266 (Tallobre et al., 2019).

267 - EF-3: Wavy and conical echo-facies showing more or less continuous and wavy
268 reflectors with the presence of conical artefacts in the deep part of the waves. In
269 comparison to EF-2, the waves are higher and their wavelengths are shorter. The conical
270 or hyperbolic seismic artefact generally attributed to a diffracting sedimentary structure

271 (Damuth, 1994), such as MTDs, or it could be a dip artefact along sediment ridges
272 associated with a complex acoustic reception induced by the wavy junction. Here, the
273 conical seismic artefact is located at the trough of wavy undulations which are
274 characterized by high amplitude (>10 m) and short wavelength (Figure 7). Thus, these
275 conical signals probably correspond to slope artefacts along sedimentary ridges
276 (Hübscher et al., 2010). Core IG-KS-08 is composed, like the cores of EF-2, of grey-
277 greenish muds and silty-sandy sediments with contouritic sequences.

278 - EF-4: Hyperbolic echo-facies characterized by small and large hyperbolic bottom
279 echoes without reflectors under the seafloor. Contrary to the previous echo-facies, this
280 one is not associated with a wavy seafloor on the bathymetry. These diffraction
281 hyperbolae can be induced by steep slopes or by the seafloor irregularity associated with
282 complex structures, such as depressions, seamounts, faults (Damuth, 1980; Lee et al.,
283 2002; Loncke et al., 2009; Sanchez-Guillamón et al., 2018), or MTD related seafloor
284 roughness (Damuth, 1980, 1994; Domzig et al., 2009; Loncke et al., 2009). These
285 artefacts make the sub-bottom profiles unusable in places and can not be eliminated by
286 processing, due to the acquisition configuration of the hull-mounted sub-bottom profiler
287 data. Those hyperbolic echo-facies have thus to be interpreted with care. Four cores (IG-
288 KS-03, IG-KS-10, IG-KS-13 and IG-KS16) recovered white indurated, low-water
289 content (30%) calcareous sediment, corresponding to Oligocene remobilized carbonates
290 (dated using the chronostratigraphic methods of strontium isotopes according to
291 McArthur et al., (2012)). Core IG-KSF-03 is located on a topographic mount on the
292 lower continental slope domain (Figure 3E). Core IG-KS-16 was collected in a SE-
293 oriented elongated scour where the Lower Miocene/Early Pliocene MTD outcrops. In
294 this case, the hyperbolae can be caused as much by structures (depression and
295 sedimentary high) as by lithology (structureless indurated carbonates).

- 296 - EF-5: Hyperbolic echo-facies expressed by small and large diffraction hyperbolae
297 overlain by thin packages of bedded reflectors. The hyperbolic echo-facies may
298 correspond to echo-facies EF-4 lately draped by stratified deposits bedded reflectors.
- 299 - EF-6: Uniform stratification above hyperbolic echo-facies, characterized by bedded and
300 continuous sub-bottom reflectors above buried hyperbolic echo-types. The hyperbolae
301 are covered by uniform stratification, probably illustrating a mass transport deposit
302 draped by hemipelagic/contouritic sedimentation. The sediment in core IG-KS-09 is
303 grey-greenish mud with silty-sandy laminae corresponding to glauconite-rich
304 contouritic sequences. The core does not reach the underlying MTD.
- 305 - EF-7: Transparent echo-facies corresponding to acoustic transparent bodies without any
306 coherent reflectors except at the base of the body. In most cases, this basal reflector
307 corresponds to an erosional surface. This echo-facies is generally associated with
308 remobilized sediments such as debris flow deposits or MTDs (Embley, 1976; Jacobi,
309 1976; Damuth, 1980; Lee et al., 2002; Domzig et al., 2009; Loncke et al., 2009;
310 Nakamura et al., 2016). On the Demerara Plateau, this transparent echo-facies has not
311 been sampled by piston cores.
- 312 - EF-8: Transparent echo-facies above uniform stratification, characterized by a
313 transparent body with an erosive base which cut bedded and continuous reflectors. It
314 illustrates a MTD which overlays and erodes older, stratified sediments. This echo-
315 facies has not been sampled.
- 316 - EF-9: Uniform stratification above transparent echo-facies, marked by a transparent
317 mass interbedded between bedded sub-bottom reflectors. It suggests a mass transport
318 deposit buried or covered by uniformly stratified sediments. The top of this echo-facies
319 has been calibrated by five cores: IG-KSF-01, 15, 17, 18 and 20. The 330 cm long IG-
320 KSF-01 collected brownish sand and grey-greenish mud from the top to 160 cm below

321 the seafloor with 43% of water content. Below 160 cm bsf the sediments are white-
322 greenish indurated carbonated muds.

323 - EF-10: Wipe-out echo-facies in association with other echo-facies, showing generally
324 more or less vertical local seismic wipe-outs (Figure 8). It is related to predominantly
325 vertical perturbations crossing the stratification in the sedimentary column. It is
326 generally interpreted as being linked to fluid ascents (gas or dewatering) (Judd and
327 Hovland, 2009; Loncke et al., 2009; Dupré et al., 2010). It mostly affects the bedded
328 EF-1 and EF-9 echo-facies (Figure 6).

329 **Echo-facies mapping**

330 **Upper Plateau**

331 This part of the plateau is characterized by bedded echo-facies EF-1 (Figure 6). The
332 bathymetric map and chirp profiles do not show particular sedimentary structures on the
333 seafloor.

334 **Intermediate Plateau to lower slope domains**

335 A great variety of echo-facies and complex distributions affects the intermediate marginal
336 plateau (Figure 5).

337 The transparent echo-facies with a uniform stratification above (EF-9) is frequent. The
338 widespread occurrence of this transparent echo-facies, interpreted as related to MTDs (Figure
339 5 and figure 6), attests to recent instabilities along the headscarp slope failure that separates the
340 upper and intermediate marginal plateaus at 1400-1600 m water depth.

341 Moreover, on the western part of the Demerara marginal plateau (W 53.00° to W 54.50°),
342 where the intermediate plateau is narrow (Figure 6), the echo-facies corresponding to MTDs is
343 also predominant. Along the headscarp slope failure, a slide (present on different sub-bottom
344 profiles) forms a tilted block in which the stratification is preserved (Figure 7).

345 On the eastern part (Figure 6, W 53° to W 51.5°), apart from the EF-1 bedded echo facies,
346 all the other echo-facies are present. The most frequent echo-facies are EF-2 (wavy bedded)
347 and EF-3 (wavy with conical artefacts; Figure 6), which correspond to stratified and undulated
348 sediment. The echo-facies with transparent signals (EF-7, EF-8 and EF-9) are concentrated along
349 the headscarp slope failure and indicate the presence of MTDs, alternating with hemipelagic
350 and contouritic sediments/deposits. A wipe-out echo facies (EF-10) is frequent between MTDs
351 and the seafloor, possibly resulting from dewatering in relation with compaction induced by
352 sediment accumulation above MTDs. On the intermediate Demerara marginal plateau, the
353 hyperbolic signals (EF-4, EF-5 and EF-6) are only present near the elongated scours alignments
354 observed on the seafloor (see figure 4 in Tallobre et al., (2016)). In these depressions (the largest
355 of which measures 4500 m long, 1800 m wide and 49 m deep), the echo-facies are transparent
356 and/or hyperbolic (Figure 9A), which is characteristic of structureless or indurated/hard, non-
357 penetrating sediments. The elongated scours, characterized by hyperbolic EF-5 echo-facies, are
358 incised into underlying transparent sedimentary highs that are nearly outcropping. Between
359 those sedimentary highs, continuously bedded facies (EF-2) characterize confined basins,
360 looking like infill drifts (Figure 9).

361 Locally, a bedded sediment accumulation is present when a structural high is present at the
362 transition from the marginal plateau to the lower continental slope (Figure 9B). There is a clear
363 continuity between the echo-facies of the intermediate and the lower marginal plateau.

364 The lower continental slope is mainly characterized by hyperbolic echo-facies EF-4 and EF-
365 5 (Figure 6). With a mean dip of 12° and a maximum dip of 20°, these hyperbolic facies
366 typically correspond to slope artefacts, making the sub-bottom profiles unexploitable in this
367 domain.

368 **Abyssal plain**

369 At the foot of the slope, the abyssal plain is characterized by a 10-20 km wide depression
370 bordered to the NE by a ~90 m high standing relief mound (Figure 10). The depressed zone is
371 composed of echo-facies EF-7, EF-8 and EF-9, illustrating the fact that the dominant deposits
372 consist of MTDs, probably originating from destabilisation of the lower continental slope. The
373 lateral relief is characterized by bedded echo-facies EF-1 and wavy bedded echo-facies EF-2
374 (Figure 6 and figure 10).

375 **Interpretation and discussion**

376 We present the main results and elements of discussion in Figure 11, which compiles (1)
377 bathymetric and oceanographic elements (Figure 11A); (2) the isopach map of Middle-
378 Pleistocene to Holocene sediments (Figure 11B) derived from the analysis of the previously
379 published and additional sub-bottom profiles (Tallobre et al., 2016) and integrated into a
380 stratigraphic framework proposed in Tallobre et al., (2019)); and (3) a simplified echo-facies
381 map (Figure 11C).

382 **Sedimentary processes on the Demerara Marginal Plateau**

383 **Upper plateau under the influence of the AAIW**

384 As demonstrated by echo-facies mapping (EF-1 continuous and bedded echo-facies) and
385 core calibration, the upper marginal plateau is mainly affected by hemipelagic sedimentation
386 (Figure 11C). Despite the fact that this part of the plateau is under the influence of the AAIW
387 water mass, no erosional features or bedforms are observed on the seafloor, either on the
388 bathymetric data or on the few sub-bottom profiles available for this part. The isopach map
389 shows that a relatively thick (up to 35 m thick) depocentre forms the very proximal domain of
390 this upper plateau (between 400 and 1200 m water depth; red patch in Figure 11B). This
391 distribution pattern is very similar to that observed by Fanget et al., (2020) at a seismic

392 resolution scale for the Plio-Quaternary. In the same way as Fanget et al., (2020), we propose
393 that the proximal and shallowest part of the upper marginal plateau is mainly under the
394 influence of terrigenous supplies from the Maroni, Oyapock and Amazon rivers. The deposits
395 progressively thin down to the intermediate plateau (1200 to ~1600 m water depth; green
396 colours, Figure 11B). On this lower part of the upper plateau we were also unable to find any
397 current-related bedforms that could reveal active contourite processes in relation to the AAIW
398 bottom current. The observations suggest that this current has no or only a negligible effect on
399 the seafloor related to its low intensity at those depths (ca. 5 cm/s at 1000 m water depth
400 according to Reid, (1989) and Peterson and Stramma, (1991)).

401 **Intermediate, lower plateau and lower continental slope under the influence of** 402 **the NADW**

403 The intermediate, lower plateau and lower continental slope show high variability in
404 sediment thicknesses and echo-facies with a general along-slope and parallel to the NADW
405 flow distribution pattern (Figure 11C). This is interpreted as reflecting the shaping effect of the
406 NADW.

407 *Moat along the headscarp slope failure*

408 Below the headscarp slope failure, the first kilometres of the intermediate marginal plateau are
409 generally characterized by thinner sediment accumulation (Figure 11B) and rougher seafloor
410 morphology (Figure 11A), suggesting erosion or non-deposition. In this area, the transparent
411 echo-facies (EF-7, EF-8 and EF-9) are present all along the headscarp slope failure (Figure
412 11C). Numerous MTDs are observed here, sometimes outcropping (EF-7, EF-8), sometimes
413 buried under contourites and hemipelagites (EF-9; fig 5). The richness in glauconitic grains in
414 cores collected in this area (Tallobre et al., 2019) indicates a low sedimentation rate related to
415 the intense winnowing generated by the bottom current on the seafloor (Giresse, 2008; Tallobre

416 et al., 2019). Therefore, this area with extremely reduced deposition seems to be characteristic
417 of a contourite channel environment (Hernández-Molina et al., 2008; Rebesco et al., 2014).
418 This part of the intermediate plateau between 1600 and 2400-2800 m water depth is interpreted
419 as a moat formed by the NADW_{sup}. It is worth noting that, despite this general tendency towards
420 erosion, some localized patchy thicker sediment accumulation zones are observed close to the
421 slope headscarp failure zone (Figure 11B). They might constitute small depocentres that formed
422 as infill and patch drifts (Tallobre et al., 2016) in relation to the NADW flowing along the
423 headscarp slope failure.

424 *Separated elongated mounded drift*

425 Downslope of the contourite channel, between ~ 2400 and 3200 m water depth, EF-2 (wavy
426 bedded) and EF-3 (wavy with conical artefacts) dominate (Figure 11C). This wavy stratification
427 is interpreted to be generated by bottom currents interacting with buried MTD ridges (Tallobre
428 et al., 2016). This bedded sediment accumulation forms an elongated along-slope drift
429 (Figure 11B) parallel to the main NADW direction. In this area, it was possible to measure
430 current velocity through an 8-month monitoring mooring in 2013 and 2014 (9.5 cm.s^{-1} on
431 average and over 30 cm.s^{-1} maximum, according to Tallobre et al., (2016)). Sediment cores
432 collected along the wavy bedded facies present graded beds with the coarsening and fining
433 upward trends typical of contourites (Gonthier et al., 1984; Stow and Faugères, 2008a; Tallobre
434 et al., 2019). This drift can be considered as a separate elongated mounded drift (Figure 7 and
435 figure 11) related to the moat guided by the updip slope failure (Faugères and Stow, 2008;
436 Rebesco et al., 2014).

437 This drift is characterized by high accumulation rates (8.8 cm/kyr Tallobre et al., (2019))
438 comparable to other drifts in the world (9 cm/kyr for the Lofoten drift: Laberg and Vorren,
439 (2004); $5 \text{ to } 13 \text{ cm/kyr}$ for the Cadiz drift: Mulder et al., (2003)). Sediments also display high

440 water content (e.g., 53% in IG-KSF-05 and IG-KS-12), which is common in drifts and may
441 explain some of the observed seismic wipe-out echo-facies (Figure 11).

442 ***Moat along the lower marginal plateau?***

443 The lower marginal plateau is characterized by very thin sediment accumulations that may
444 be interpreted as erosion or non-deposition (Figure 11B). The geometry of reflectors (Figure
445 12) is not really conclusive: sediment layers progressively thin distally (Figure 12), which may
446 suggest no deposition. This domain is characterized by EF-2 (wavy bedded), EF-6 (bedded
447 above transparent) and EF-9 (bedded above hyperbolae) echo-facies (Figure 11C and figure
448 12). Rare thick depocentres are localized on the lower plateau (Figure 11B, red colours on the
449 lower plateau and figure 9). These depocentres may be considered as infill drifts emplaced close
450 to local reliefs (Laberg et al., 2001; Rebesco, 2005; Rebesco et al., 2014). This area is probably
451 under NADW_{inf} influence, whose velocity is relatively high in tropical areas, around 20.3 cm/s
452 (Reid, 1989; Tsuchiya et al., 1994; Mauritzen et al., 2002), and the observed low sediment
453 accumulation may be caused by the winnowing effects of bottom currents. The lower plateau
454 may be interpreted as another moat formed by the NADW_{inf}.

455 ***Steep and eroded lower continental slope***

456 The lower continental slope is characterized by a high slope value (12° on average) and by
457 EF-4 hyperbolic facies, typically interpreted as seismic artefacts related to the slope (Figure 7
458 and figure 11C). Seismic data analysis shows that this slope is an eroded or non-deposition area
459 (Pattier et al., 2013). We think that the high-velocity NADW_{inf} promotes slope instability.

460 ***Abyssal plain under the influence of the AABW***

461 The abyssal plain is composed of two distinct areas: the Demerara abyssal plain north of the
462 Demerara Plateau and the Guiana abyssal plain east of the Demerara Plateau (Figure 2A and
463 Figure 11).

464 (1) In the Demerara abyssal plain, echo-facies show an along-slope distribution with, at the
465 foot of the marginal plateau, a 20 km wide depression where transparent echo-facies EF-
466 7 and EF-8 and uniform stratification above transparent echo-facies EF-9 dominate
467 (Figure 10 and figure 11C). These transparent echo-facies clearly relate to successive
468 MTDs (Figure 10) that probably originate from the destabilization of the steep lower
469 continental slope. Northward, bedded echo-facies EF-1 dominates in the form of a
470 mounded sedimentary accumulation (Figure 10 and figure 11). Sediment waves are
471 observed towards the north of the mound (Figure 10). Directly along the slope, this area
472 with MTD accumulation corresponds to a contourite moat whereas the presence of
473 bedded deposit corresponds to an elongated mounded drift which evolves in a sheeted
474 drift northward. This architecture is similar to the drift observed in the Cadix abyssal
475 plain (Llave et al., (2001). Contrary to the intermediate and lower marginal plateaus,
476 which are under the NADW influence, the abyssal plain is under the AABW influence,
477 as previously described in Gonthier et al., (2002) and in Loncke et al., (2009). Lateral
478 horizon picking shows that accumulation can be thicker in the moat than on the drift
479 (Figure 10), a paradox related to the recurrent instability of the lower continental slope,
480 infilling the moat with successive MTDs and balancing erosion.

481 (2) In the Guiana abyssal plain, a thick sediment accumulation (exceeding 33 m,
482 Figure 11B) occurs and echo-facies are bedded (EF-1) and bedded above transparent
483 (EF-9). Two reasons might be advocated to explain these thick sediment accumulations:
484 (i) the presence of Guianese canyons clearly visible on the bathymetry (detail on Figure
485 3F and figure 11A, southwestern corner of the map) that possibly channel the sediment
486 down to this area, and also (ii) the lateral advection related to the NADW sediment
487 transport. This strong accumulation may partly correspond to a NADW derived
488 contourite sedimentary fan (Figure 11).

489 **Influence of water mass related instabilities on the sedimentary record**

490 The Demerara plateau and abyssal plain are the locus of at least two CDS related respectively
491 to the NADW and the AABW. In both cases, slope instability plays an important role in
492 sedimentary patterns:

493 (1) On the Demerara “NADW CDS” plateau, the main instability initiates along the
494 headscarp slope failure that localizes the edge of the NADW moat. Generally, along the
495 contouritic channels, erosion caused by the winnowing effect can change pressure
496 conditions in the sedimentary column. This leads to a decrease in cohesion and friction
497 forces and then to slope instability (Ingram et al., 2011). Hence, the erosion in the moats,
498 along the headscarp slope failure and on the lower marginal plateau, can contribute to
499 promote regular instabilities and mass-wasting along the slope failure headscarp and
500 along the lower continental slope. The slope variations between the upper marginal
501 plateau (1°) and the intermediate marginal plateau (3°) can also promote the
502 maintenance of instability through time by retrogressive erosion. In addition, the
503 transition from the upper to the intermediate plateau corresponds to the transition from
504 AAIW to NADW, highly contrasting in salinity and temperature. In such a context, the
505 formation of internal waves may occur, which oscillate at and under this interface, called
506 a pycnocline (Sandstrom and Elliott, 1984; Shanmugam, 2013). On the Demerara
507 Plateau, the internal waves are associated with the semi-diurnal tidal signal, with a
508 period of 12.42 h (Tallobre et al., 2016). This phenomenon promotes erosion and
509 sediment transport (de Madron et al., 1999; Puig et al., 2004). The sum of NADW
510 erosion along the moat, internal wave break and slope steepness likely explains the
511 recurrent instability and the initiation of numerous MTDs along the upper NADW moat.

512 (2) In the Demerara abyssal plain, the AABW moat forms an elongated depression at the
513 foot of the plateau (Figure 10). This moat is infilled with an alternation of bedded and

514 transparent sediments interpreted as a stacking of contourites and MTDs originating
515 from the recurrent destabilization of the steep lower continental slope. This sedimentary
516 pattern is very well expressed on the echo-facies map (Figure 11C) with transparent
517 moat echo-facies highly contrasting with the drift bedded echo-facies.

518 To conclude, MTDs are numerous on the Demerara marginal plateau in the CDSs linked to
519 the NADW and AABW. These MTDs are either related to the longitudinal erosion power of
520 those contour-parallel thermohaline currents regularly reactivating slides along steep slope
521 domains, or to the breaking of internal waves.

522 Such observations have been made in many other CDSs around the world: along the
523 Argentine slope (Hernández-Molina et al., 2009), on the Pianosa ridge (Cattaneo et al., 2014),
524 along the Adriatic Margin (Verdicchio et al., 2007), in the Bay of Biscay (Faugères et al., 2002),
525 on the Vøring plateau (Orvik and Niiler, 2002; Laberg et al., 2005; Hernández-Molina et al.,
526 2008) and many other examples quoted in Laberg and Camerlenghi, (2008).

527 **Using the sub-bottom profiler to characterize contourites**

528 Considering their penetration range (the first hundred metres of sediment, depending on
529 sediment type) and average vertical resolution (commonly 20 to 40 cm), sub-bottom profiles
530 are well suited for imaging recent sedimentary patterns (depending on sedimentation rates,
531 Pleistocene to Holocene time frames) and understanding associated palaeoceanographic
532 archives. Therefore, this type of geophysical data is frequently combined with core data to
533 analyse recent sedimentary deposits and processes.

534 Our study combines echo-facies mapping with calibration by sediment cores and enables us
535 to propose some CDS recognition criteria:

536 (1) Contourite drifts are clearly expressed on echo-facies maps by along-slope, slope-
537 parallel distribution patterns of echo-facies (Figure 11C). Echo-facies are dominantly
538 depositional types, sometimes with wave-like bedforms (bedded, wavy bedded or wavy

539 and conical echo-facies). Wipe-out echo-facies frequently affect the bedded echo-facies
540 within drifts, possibly resulting from high water content or organic contents typical of
541 drifts (Laberg and Camerlenghi, 2008; Wetzel et al., 2008).

542 (2) Moats are expressed by echo-facies typical of erosion, non-deposition, exposed
543 indurated slopes or slope instability (hyperbolic, transparent or alternations of bedded
544 and transparent echo-facies) by opposition to drifts.

545 (3) On isopach maps, moats and contouritic channels are depleted domains compared to
546 drifts (Figure 11B). On the Demerara Plateau, the NADW elongated mounded drift is
547 characterized by an along-slope, slope-parallel depocentre disconnected from upslope
548 sediment depocentres by an along-slope depleted moat corridor. At the foot of the
549 Demerara Plateau, the contrast in thickness between the AABW moat and its related
550 elongated mounded drift is sometimes less clear due to MTD infills in the moat
551 (Figure 10), but the association with the echo-facies enables us to evidence contourite
552 processes.

553 (4) At a more local scale, infill drifts related to local topographic variations (mini-basins
554 between outcropping MTDs or basement ridges) (Figure 11) are clearly expressed on
555 isopach maps as thickly sedimented patches (Figure 11B).

556 **Conclusion**

557 This paper presents a new, comprehensive and up-to-date echo-facies map of Contourite
558 Depositional Systems along the Demerara marginal plateau and abyssal plain in relation with
559 the NADW and AABW thermohaline deep currents.

560 These CDSs display moats characterized by hyperbolic, transparent and bedded transparent
561 echo-facies related to strong erosion and slope instability. In turn, the depositional drifts are
562 characterized by bedded to undulated-bedded echo-facies related to contourite accumulations
563 and associated depositional bedforms. In these drifts, seismic wipe-outs are frequent and attest

564 to high fluid content. The hyperbolic echo-facies occurs where MTDs are exposed by the
565 activity of bottom currents (either eroding or preventing sedimentation).

566 The echo-facies map shows typical along-slope patterns that correlate with isopach map
567 thickness variations, enhancing the fact that the combination of these approaches is very
568 efficient for contourite recognition at a regional scale:

- 569 - Moats correspond to along-slope elongated depleted zones displaying the
570 hyperbolic, transparent and transparent bedded echo-facies typical of erosion, non-
571 deposition, exposed slopes or slope instability,
- 572 - Drifts correspond to along-slope elongated depocentres displaying bedded, wavy
573 bedded echo-facies with internal depositional bedforms and frequent seismic wipe-
574 outs probably related to high fluid contents.

575

576 **Acknowledgments**

577 We sincerely thank David Graindorge, Frauke Klingelhoefer and Christophe Basile for
578 having given access to sub-bottom profiler data acquired during the MARGATS and
579 DRADEM cruises. We thank Shell and Ifremer for the funding of Cedric Tallobre's PhD.

580 **References**

581 **Uncategorized References**

- 582 Bahk, J. J., S. H. Lee, H. S. Yoo, G. G. Back, and S. K. Chough, 2005, Late Quaternary
583 sedimentary processes and variations in bottom-current activity in the Ulleung
584 Interplain Gap, East Sea (Korea): *Marine Geology*, **217**, no. 1, 119-142.
585 <http://dx.doi.org/https://doi.org/10.1016/j.margeo.2005.02.031>.
- 586 Basile, C., 2016, DRADEM cruise, RV Pourquoi pas?
- 587 Basile, C., A. Maillard, M. Patriat, V. Gaullier, L. Loncke, W. Roest, M. Mercier de Lépinay,
588 and F. Pattier, 2013, Structure and evolution of the Demerara Plateau, offshore French
589 Guiana: Rifting, tectonic inversion and post-rift tilting at transform–divergent margins
590 intersection: *Tectonophysics*, **591**, no. 0, 16-29.
591 <http://dx.doi.org/http://dx.doi.org/10.1016/j.tecto.2012.01.010>.
- 592 Cattaneo, A., G. Jouet, S. Charrier, E. Théreau, and V. Riboulot, 2014, Submarine landslides
593 and contourite drifts along the Pianosa Ridge (Corsica Trough, Mediterranean Sea),
594 *Submarine Mass Movements and Their Consequences*: Springer, 435-445.
- 595 Damuth, J. E., 1980, Use of high-frequency (3.5–12 kHz) echograms in the study of near-
596 bottom sedimentation processes in the deep-sea: A review: *Marine Geology*, **38**, no. 1–
597 3, 51-75. [http://dx.doi.org/http://dx.doi.org/10.1016/0025-3227\(80\)90051-1](http://dx.doi.org/http://dx.doi.org/10.1016/0025-3227(80)90051-1).
- 598 Damuth, J. E., 1994, Neogene gravity tectonics and depositional processes on the deep Niger
599 Delta continental margin: *Marine and Petroleum Geology*, **11**, no. 3, 320-346.
600 [http://dx.doi.org/http://dx.doi.org/10.1016/0264-8172\(94\)90053-1](http://dx.doi.org/http://dx.doi.org/10.1016/0264-8172(94)90053-1).
- 601 de Lépinay, M. M., L. Loncke, C. Basile, W. R. Roest, M. Patriat, A. Maillard, and P. De
602 Clarens, 2016, Transform continental margins–Part 2: A worldwide review:
603 *Tectonophysics*, **693**, 96-115.
- 604 de Madron, X. D., P. Castaing, F. Nyffeler, and T. Courp, 1999, Slope transport of suspended
605 particulate matter on the Aquitanian margin of the Bay of Biscay: *Deep Sea Research*
606 *Part II: Topical Studies in Oceanography*, **46**, no. 10, 2003-2027.
- 607 Domzig, A., V. Gaullier, P. Giresse, H. Pauc, J. Déverchère, and K. Yelles, 2009, Deposition
608 processes from echo-character mapping along the western Algerian margin (Oran–
609 Tenes), Western Mediterranean: *Marine and Petroleum Geology*, **26**, no. 5, 673-694.
610 <http://dx.doi.org/https://doi.org/10.1016/j.marpetgeo.2008.05.006>.
- 611 Ducassou, E., L. Fournier, F. J. Sierro, C. A. Alvarez Zarikian, J. Lofi, J. A. Flores, and C.
612 Roque, 2016, Origin of the large Pliocene and Pleistocene debris flows on the Algarve
613 margin: *Marine Geology*, **377**, 58-76.
614 <http://dx.doi.org/http://dx.doi.org/10.1016/j.margeo.2015.08.018>.
- 615 Dupré, S., J. Woodside, I. Klauke, J. Mascle, and J.-P. Foucher, 2010, Widespread active
616 seepage activity on the Nile Deep Sea Fan (offshore Egypt) revealed by high-definition
617 geophysical imagery: *Marine Geology*, **275**, no. 1, 1-19.
618 <http://dx.doi.org/https://doi.org/10.1016/j.margeo.2010.04.003>.
- 619 Embley, R., 1976, New evidence for occurrence of debris-flow deposits in the deep-sea.:
620 *Geology*, **4**, 371-374.
- 621 Enjorlas, J. M., J. Gouadain, E. Mutti, and J. Pizon, 1986, New turbiditic model for the Lower
622 Tertiary sands in the South Viking Graben, *in* A. M. Spencer, ed., *Habitat of*
623 *Hydrocarbons on the Norwegian Continental Shelf*: Norwegian Petroleum Society, 171-
624 178.

- 625 Fanget, A.-S., L. Loncke, F. Pattier, T. Marsset, W. R. Roest, C. Tallobre, X. Durrieu de
626 Madron, and F. J. Hernández-Molina, 2020, A synthesis of the sedimentary evolution
627 of the Demerara Plateau (Central Atlantic Ocean) from the late Albian to the Holocene:
628 Marine and Petroleum Geology, **114**, 104195.
629 <http://dx.doi.org/https://doi.org/10.1016/j.marpetgeo.2019.104195>.
- 630 Faugères, J.-C., E. Gonthier, T. Mulder, N. Kenyon, P. Cirac, R. Griboulard, S. Berné, and R.
631 Lesuavé, 2002, Multi-process generated sediment waves on the Landes Plateau (Bay of
632 Biscay, North Atlantic): Marine Geology, **182**, no. 3–4, 279-302.
633 [http://dx.doi.org/http://dx.doi.org/10.1016/S0025-3227\(01\)00242-0](http://dx.doi.org/http://dx.doi.org/10.1016/S0025-3227(01)00242-0).
- 634 Faugères, J. C., and D. A. V. Stow, 2008, Chapter 14 Contourite Drifts: Nature, Evolution and
635 Controls, in M. Rebesco, and A. Camerlenghi, eds., Developments in sedimentology:
636 Elsevier, 257-288.
- 637 Faugères, J. C., and T. Mulder, 2011, Contour Currents and Contourite Drifts: in: Heiko Hüneke
638 and Thierry Mulder, Deep sea sediments, Elsevier publications, developments in
639 sedimentology, **63**, 149-205.
- 640 Giresse, P., 2008, Chapter 12 Some Aspects of Diagenesis in Contourites, in M. Rebesco, and
641 A. Camerlenghi, eds., Developments in sedimentology: Elsevier, 203-221.
- 642 Gonthier, E., J. C. Faugères, and D. A. V. Stow, 1984, Contourite facies of the Faro drift:
643 Geological society of London, special publication, **15**, 275-292.
- 644 Gonthier, E., J. C. Faugères, A. Gervais, G. Ercilla, B. Alonso, and J. Baraza, 2002, Quaternary
645 sedimentation and origin of the Orinoco sediment-wave field on the Demerara
646 continental rise (NE margin of South America): Marine Geology, **192**, no. 1–3, 189-
647 214. [http://dx.doi.org/http://dx.doi.org/10.1016/S0025-3227\(02\)00555-8](http://dx.doi.org/http://dx.doi.org/10.1016/S0025-3227(02)00555-8).
- 648 Gouyet, S., 1988, Evolution tectono-sédimentaire des marges guyanaise et nordbrésilienne au
649 cours de l'ouverture de l'Atlantique Sud., Université de Pau.
- 650 Graindorge, D., and F. Klingelhofer. 2016, MARGATS cruise, RV L'Atalante,.
- 651 Hanquiez, V., T. Mulder, S. Toucanne, P. Lecroart, C. Bonnel, E. Marchès, and E. Gonthier,
652 2010, The sandy channel-lobe depositional systems in the Gulf of Cadiz: Gravity
653 processes forced by contour current processes: Sedimentary Geology, **229**, no. 3, 110-
654 123. <http://dx.doi.org/http://dx.doi.org/10.1016/j.sedgeo.2009.05.008>.
- 655 Heezen, B. C., 1959, Dynamic Processes of Abyssal Sedimentation: Erosion, Transportation,
656 and Redeposition on the Deep-sea floor: Geophysical Journal International, **2**, no. 2,
657 142-163. <http://dx.doi.org/10.1111/j.1365-246X.1959.tb05790.x>.
- 658 Heezen, B. C., and G. L. Johnson, 1963, A moated knoll in the Canary Passage.: Dent.
659 Hydrograph. Z., **16**, no. 6, 269-272.
- 660 Heezen, B. C., and C. Hollister, 1964, Deep-sea current evidence from abyssal sediments:
661 Marine Geology, **1**, no. 2, 141-174. [http://dx.doi.org/http://dx.doi.org/10.1016/0025-
662 3227\(64\)90012-X](http://dx.doi.org/http://dx.doi.org/10.1016/0025-3227(64)90012-X).
- 663 Hernández-Molina, F. J., E. Llave, and D. A. V. Stow, 2008, Chapter 19 Continental Slope
664 Contourites, in M. Rebesco, and A. Camerlenghi, eds., Developments in sedimentology:
665 Elsevier, 379-408.
- 666 Hernández-Molina, F. J., M. Paterlini, R. Violante, P. Marshall, M. de Isasi, L. Somoza, and
667 M. Rebesco, 2009, Contourite depositional system on the Argentine Slope: An
668 exceptional record of the influence of Antarctic water masses: Geology, **37**, no. 6, 507-
669 510. <http://dx.doi.org/10.1130/g25578a.1>.
- 670 Herold, N., M. Huber, R. Müller, and M. Seton, 2012, Modeling the Miocene climatic optimum:
671 Ocean circulation: Paleoceanography, **27**, no. 1.

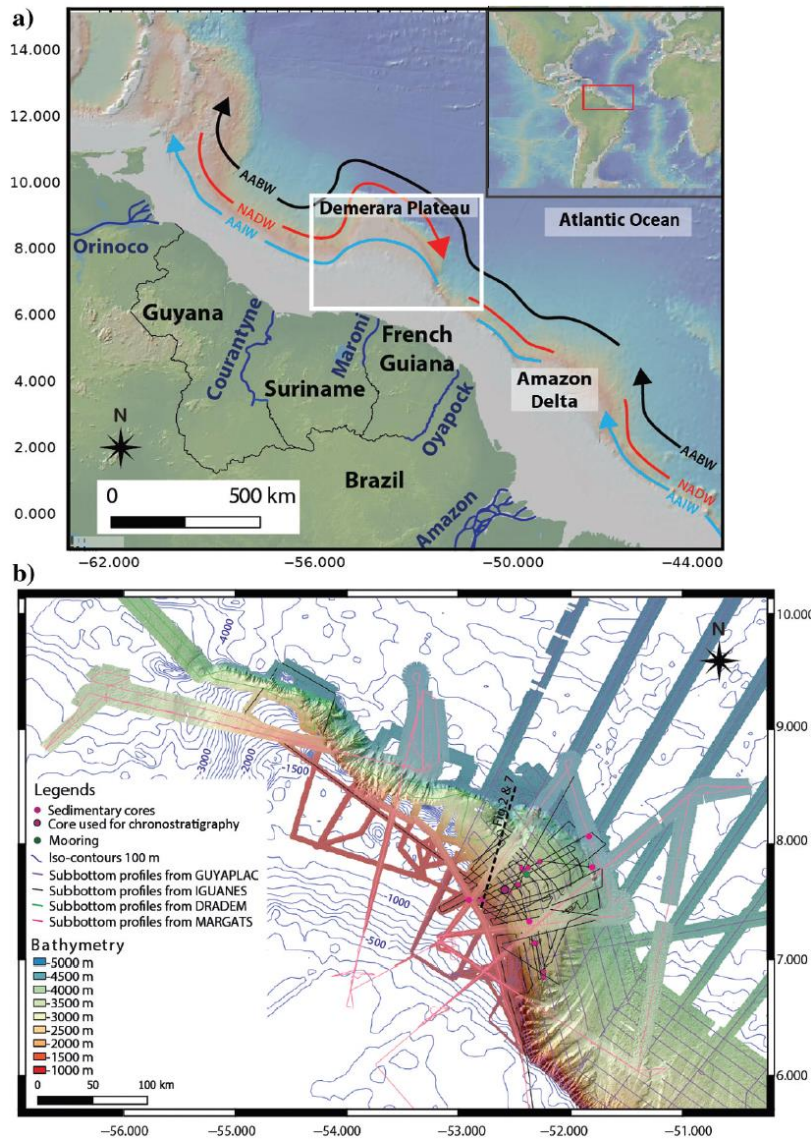
- 672 Hogg, N. G., 1997, The Deep Basin Experiment - status and accomplishments. : WOCE South
673 Atlantic Workshop.
- 674 Hübscher, C., C. Dullo, S. Flögel, J. Titschack, and J. Schönfeld, 2010, Contourite drift
675 evolution and related coral growth in the eastern Gulf of Mexico and its gateways:
676 International Journal of Earth Sciences, **99**, no. 1, 191-206.
- 677 Ingram, W. C., D. C. Mosher, and S. W. J. Wise, 2011, Biostratigraphy of an upper Miocene
678 mass transport deposit on Demerara Rise, northern South American margin, *in* C. Shipp,
679 P. Weimer, and H. Posamentier, eds., Mass-transport Deposits in Deepwater Settings:
680 SEPM Special Publication 96, 457-498.
- 681 Jacobi, R. D., 1976, Sediment slides on the northwestern continental margin of Africa: Marine
682 Geology, **22**, no. 3, 157-173.
- 683 Johns, W. E., D. M. Fratantoni, and R. J. Zantopp, 1993, Deep western boundary current
684 variability off northeastern Brazil: Deep Sea Research Part I: Oceanographic Research
685 Papers, **40**, no. 2, 293-310. [http://dx.doi.org/http://dx.doi.org/10.1016/0967-
686 0637\(93\)90005-N](http://dx.doi.org/http://dx.doi.org/10.1016/0967-0637(93)90005-N).
- 687 Judd, A., and M. Hovland, 2009, Seabed fluid flow: the impact on geology, biology and the
688 marine environment: Cambridge University Press.
- 689 Knutz, P. C., 2008, Chapter 24 Palaeoceanographic Significance of Contourite Drifts, *in* M.
690 Rebesco, and A. Camerlenghi, eds., Developments in sedimentology: Elsevier, 511-
691 535.
- 692 Koltermann, K. P., V. Gouretski, and K. Jancke, 2011, Hydrographic Atlas of the World Ocean
693 Circulation Experiment (WOCE): Volume 3: Atlantic Ocean: National Oceanography
694 Centre.
- 695 Laberg, J. S., and T. O. Vorren, 2004, Weichselian and Holocene growth of the northern high-
696 latitude Lofoten Contourite Drift on the continental slope of Norway: Sedimentary
697 Geology, **164**, no. 1-2, 1-17.
698 <http://dx.doi.org/http://dx.doi.org/10.1016/j.sedgeo.2003.07.004>.
- 699 Laberg, J. S., and A. Camerlenghi, 2008, Chapter 25 The Significance of Contourites for
700 Submarine Slope Stability, *in* M. Rebesco, and A. Camerlenghi, eds., Developments in
701 sedimentology: Elsevier, 537-556.
- 702 Laberg, J. S., K. I. T. Dahlgren, and T. O. Vorren, 2005, The Eocene-late Pliocene
703 paleoenvironment in the Vøring Plateau area, Norwegian Sea—paleoceanographic
704 implications: Marine Geology, **214**, no. 1-3, 269-285.
705 <http://dx.doi.org/http://dx.doi.org/10.1016/j.margeo.2004.10.031>.
- 706 Laberg, J. S., T. Dahlgren, T. O. Vorren, H. Haflidason, and P. Bryn, 2001, Seismic analyses
707 of Cenozoic contourite drift development in the Northern Norwegian Sea: Marine
708 Geophysical Researches, **22**, no. 5, 401-416.
709 <http://dx.doi.org/10.1023/a:1016347632294>.
- 710 Le Suave, R., and P. Beuzart, 2003, GUYAPLAC cruise, RV L'Atalante.
- 711 Lee, H. J., J. P. M. Syvitski, G. Parker, D. Orange, J. Locat, E. W. H. Hutton, and J. Imran,
712 2002, Distinguishing sediment waves from slope failure deposits: field examples,
713 including the 'Humboldt slide', and modelling results: Marine Geology, **192**, no. 1-3,
714 79-104. [http://dx.doi.org/http://dx.doi.org/10.1016/S0025-3227\(02\)00550-9](http://dx.doi.org/http://dx.doi.org/10.1016/S0025-3227(02)00550-9).
- 715 Llave, E., F. J. Hernández-Molina, L. Somoza, V. Díaz-del-Río, D. A. V. Stow, A. Maestro,
716 and J. M. Alveirinho Dias, 2001, Seismic stacking pattern of the Faro-Albufeira
717 contourite system (Gulf of Cadiz): a Quaternary record of paleoceanographic and

- 718 tectonic influences: *Marine Geophysical Researches*, **22**, no. 5, 487-508.
719 <http://dx.doi.org/10.1023/a:1016355801344>.
- 720 Loncke, L., 2013, IGUANES, RV L'Atalante.
- 721 Loncke, L., L. Droz, V. Gaullier, C. Basile, M. Patriat, and W. Roest, 2009, Slope instabilities
722 from echo-character mapping along the French Guiana transform margin and Demerara
723 abyssal plain: *Marine and Petroleum Geology*, **26**, no. 5, 711-723.
724 <http://dx.doi.org/http://dx.doi.org/10.1016/j.marpetgeo.2008.02.010>.
- 725 Loncke, L., W. R. Roest, F. Klingelhoefer, C. Basile, D. Graindorge, A. Heuret, B. Marcaillou,
726 T. Museur, A. S. Fanget, and M. Mercier de Lépinay, 2020, Transform Marginal
727 Plateaus: *Earth-Science Reviews*, **203**, 102940.
728 <http://dx.doi.org/https://doi.org/10.1016/j.earscirev.2019.102940>.
- 729 Loncke, L., A. Maillard, C. Basile, W. R. Roest, G. Bayon, V. Gaullier, F. Pattier, M. Mercier
730 de Lépinay, C. Grall, L. Droz, T. Marsset, P. Giresse, J. C. Caprais, C. Cathalot, D.
731 Graindorge, A. Heuret, J. F. Lebrun, S. Bermell, B. Marcaillou, C. Sotin, B. Hebert, M.
732 Patriat, M. A. Bassetti, C. Tallobre, R. Buscail, X. Durrieu de Madron, and F. Bourrin,
733 2016, Structure of the Demerara passive-transform margin and associated sedimentary
734 processes. Initial results from the IGUANES cruise: Geological Society, London,
735 Special Publications, **431**. <http://dx.doi.org/10.1144/sp431.7>.
- 736 Mauritzen, C., K. L. Polzin, M. S. McCartney, R. C. Millard, and D. E. West-Mack, 2002,
737 Evidence in hydrography and density fine structure for enhanced vertical mixing over
738 the Mid-Atlantic Ridge in the western Atlantic: *Journal of Geophysical Research:*
739 *Oceans*, **107**, no. C10, 3147-3166.
- 740 McArthur, J. M., R. J. Howarth, and G. A. Shields, 2012, Chapter 7 - Strontium Isotope
741 Stratigraphy, *The Geologic Time Scale*: Elsevier, 127-144.
- 742 Mercier de Lépinay, M., 2016, Inventaire mondial des marges transformantes et évolution
743 tectono-sédimentaire des plateaux de Demerara et de Guinée, Université de Perpignan
744 Via Domitia.
- 745 Mercier de Lépinay, M., L. Loncke, C. Basile, W. Roest, M. Patriat, A. Maillard, and P. De
746 Clarens, 2016, Transform continental margins - Part 2: A worldwide inventory:
747 *Tectonophysics*, **693**.
- 748 Molinari, R. J., R. A. Fine, and J. E., 1992, The Deep Western Boundary Current in the tropical
749 North Atlantic Ocean: *Deep Sea Research*, **39**, no. 11/12, 1967-1984.
- 750 Mulder, T., M. Voisset, P. Lecroart, E. Le Drezen, E. Gonthier, V. Hanquiez, J.-C. Faugères,
751 E. Habgood, F. J. Hernandez-Molina, F. Estrada, E. Llave-Barranco, D. Poirier, C.
752 Gorini, Y. Fuchey, A. Voelker, P. Freitas, F. L. Sanchez, L. M. Fernandez, N. H.
753 Kenyon, and J. Morel, 2003, The Gulf of Cadiz: an unstable giant contouritic levee:
754 *Geo-Marine Letters*, **23**, no. 1, 7-18. <http://dx.doi.org/10.1007/s00367-003-0119-0>.
- 755 Nakamura, K., S. Machida, K. Okino, Y. Masaki, K. Iijima, K. Suzuki, and Y. Kato, 2016,
756 Acoustic characterization of pelagic sediments using sub-bottom profiler data:
757 Implications for the distribution of REY-rich mud in the Minamitorishima EEZ, western
758 Pacific: *Geochemical Journal*, **50**, no. 6, 605-619.
- 759 Niemi, T. M., Z. Ben-Avraham, C. J. Hartnady, and M. Reznikov, 2000, Post-Eocene seismic
760 stratigraphy of the deep ocean basin adjacent to the southeast African continental
761 margin: a record of geostrophic bottom current systems: *Marine Geology*, **162**, no. 2-4,
762 237-258.

- 763 Orvik, K. A., and P. Niiler, 2002, Major pathways of Atlantic water in the northern North
764 Atlantic and Nordic Seas toward Arctic: *Geophysical Research Letters*, **29**, no. 19, 1896.
765 <http://dx.doi.org/10.1029/2002GL015002>.
- 766 Pattier, F., L. Loncke, P. Imbert, V. Gaullier, C. Basile, A. Maillard, W. R. Roest, M. Patriat,
767 and B. C. Vendeville, 2015, Origin of an enigmatic regional Mio-Pliocene unconformity
768 on the Demerara plateau: *Marine Geology*, **365**, no. 0, 21-35.
769 <http://dx.doi.org/http://dx.doi.org/10.1016/j.margeo.2015.04.001>.
- 770 Pattier, F., L. Loncke, V. Gaullier, C. Basile, A. Maillard, P. Imbert, W. R. Roest, B. C.
771 Vendeville, M. Patriat, and B. Loubrieu, 2013, Mass-transport deposits and fluid
772 venting in a transform margin setting, the eastern Demerara Plateau (French Guiana):
773 *Marine and Petroleum Geology*, **46**, no. 0, 287-303.
774 <http://dx.doi.org/http://dx.doi.org/10.1016/j.marpetgeo.2013.06.010>.
- 775 Peterson, R. G., and L. Stramma, 1991, Upper-level circulation in the South Atlantic Ocean:
776 *Progress in Oceanography*, **26**, no. 1, 1-73.
777 [http://dx.doi.org/http://dx.doi.org/10.1016/0079-6611\(91\)90006-8](http://dx.doi.org/http://dx.doi.org/10.1016/0079-6611(91)90006-8).
- 778 Pfuhl, H. A., and I. N. McCave, 2005, Evidence for late Oligocene establishment of the
779 Antarctic Circumpolar Current: *Earth and Planetary Science Letters*, **235**, no. 3-4, 715-
780 728.
- 781 Puig, P., A. Palanques, J. Guillén, and M. El Khatab, 2004, Role of internal waves in the
782 generation of nepheloid layers on the northwestern Alboran slope: Implications for
783 continental margin shaping: *Journal of Geophysical Research: Oceans*, **109**, no. C9,
784 C09011. <http://dx.doi.org/10.1029/2004JC002394>.
- 785 Rebesco, M., 2005, SEDIMENTARY ENVIRONMENTS | Contourites, in R. C. S. R. M. C.
786 R. Plimer, ed., *Encyclopedia of Geology*: Elsevier, 513-527.
- 787 Rebesco, M., F. J. Hernández-Molina, D. Van Rooij, and A. Wåhlin, 2014, Contourites and
788 associated sediments controlled by deep-water circulation processes: State-of-the-art
789 and future considerations: *Marine Geology*, **352**, no. 0, 111-154.
790 <http://dx.doi.org/http://dx.doi.org/10.1016/j.margeo.2014.03.011>.
- 791 Reid, J. L., 1989, On the total geostrophic circulation of the South Atlantic Ocean: Flow
792 patterns, tracers, and transports: *Progress in Oceanography*, **23**, no. 3, 149-244.
793 [http://dx.doi.org/http://dx.doi.org/10.1016/0079-6611\(89\)90001-3](http://dx.doi.org/http://dx.doi.org/10.1016/0079-6611(89)90001-3).
- 794 Sanchez-Guillamón, O., J. T. Vázquez, D. Palomino, T. Medialdea, L. M. Fernández-Salas, R.
795 León, and L. Somoza, 2018, Morphology and shallow structure of seafloor mounds in
796 the Canary Basin (Eastern Central Atlantic Ocean): *Geomorphology*, **313**, 27-47.
797 <http://dx.doi.org/https://doi.org/10.1016/j.geomorph.2018.04.007>.
- 798 Sandstrom, H., and J. Elliott, 1984, Internal tide and solitons on the Scotian Shelf: A nutrient
799 pump at work: *Journal of Geophysical Research: Oceans*, **89**, no. C4, 6415-6426.
- 800 Shanmugam, G., 2013, New perspectives on deep-water sandstones: Implications: *Petroleum*
801 *Exploration and Development*, **40**, no. 3, 316-324.
802 [http://dx.doi.org/http://dx.doi.org/10.1016/S1876-3804\(13\)60038-5](http://dx.doi.org/http://dx.doi.org/10.1016/S1876-3804(13)60038-5).
- 803 Stow, D., and J.-C. Faugères, 2008a, Contourite facies and the facies model: Developments in
804 sedimentology, **60**, 223-256.
- 805 Stow, D. A. V., and J. C. Faugères, 2008b, Chapter 13 Contourite Facies and the Facies Model,
806 in M. Rebesco, and A. Camerlenghi, eds., *Developments in sedimentology*: Elsevier,
807 223-256.

- 808 Stramma, L., and F. Schott, 1999, The mean flow field of the tropical Atlantic Ocean: Deep Sea
809 Research Part II: Topical Studies in Oceanography, **46**, no. 1–2, 279-303.
810 [http://dx.doi.org/http://dx.doi.org/10.1016/S0967-0645\(98\)00109-X](http://dx.doi.org/http://dx.doi.org/10.1016/S0967-0645(98)00109-X).
- 811 Suga, T., and L. D. Talley, 1995, Antarctic Intermediate Water circulation in the tropical and
812 subtropical South Atlantic: Journal of Geophysical Research: Oceans, **100**, no. C7,
813 13441-13453. <http://dx.doi.org/10.1029/95JC00858>.
- 814 Tallobre, C., 2017, Mise en évidence d'un système de dépôt contouritique et des processus
815 sédimentaires associés sur le plateau de Demerara (marge guyanaise), Université de
816 Perpignan via Domitia.
- 817 Tallobre, C., P. Giresse, M.-A. Bassetti, L. Loncke, G. Bayon, R. Buscail, A. Tudryn, and S.
818 Zaragosi, 2019, Formation and evolution of glauconite in the Demerara Contourite
819 depositional system related to NADW circulation changes during late Quaternary
820 (French Guiana): Journal of South American Earth Sciences, **92**, 167-183.
821 <http://dx.doi.org/https://doi.org/10.1016/j.jsames.2019.03.011>.
- 822 Tallobre, C., L. Loncke, M.-A. Bassetti, P. Giresse, G. Bayon, R. Buscail, X. D. de Madron, F.
823 Bourrin, M. Vanhaesebroucke, and C. Sotin, 2016, Description of a contourite
824 depositional system on the Demerara Plateau: Results from geophysical data and
825 sediment cores: Marine Geology, **378**, 56-73.
826 <http://dx.doi.org/http://dx.doi.org/10.1016/j.margeo.2016.01.003>.
- 827 Tsuchiya, M., L. D. Talley, and M. S. McCartney, 1994, Water-mass distributions in the
828 western South Atlantic; A section from South Georgia Island (54°S) northward across
829 the equator.: Journal of Marine Research, **52**, 51-81.
- 830 Uenzelmann-Neben, G., T. Weber, J. Gruetzner, and M. Thomas, 2017, Transition from the
831 Cretaceous ocean to Cenozoic circulation in the western South Atlantic—A twofold
832 reconstruction: Tectonophysics, **716**, 225-240.
- 833 Unternehr, P., D. Curie, J. Olivet, J. Goslin, and P. Beuzart, 1988, South Atlantic fits and
834 intraplate boundaries in Africa and South America: Tectonophysics, **155**, no. 1-4, 169-
835 179.
- 836 Verdicchio, G., F. Trincardi, and A. Asioli, 2007, Mediterranean bottom-current deposits: an
837 example from the Southwestern Adriatic Margin: Geological Society, London, Special
838 Publications, **276**, no. 1, 199-224.
- 839 Viana, A. R., 2008, Chapter 23 Economic Relevance of Contourites, *in* M. Rebesco, and A.
840 Camerlenghi, eds., Developments in sedimentology: Elsevier, 491-510.
- 841 Wetzel, A., F. Werner, and D. A. V. Stow, 2008, Chapter 11 Bioturbation and Biogenic
842 Sedimentary Structures in Contourites, *in* M. Rebesco, and A. Camerlenghi, eds.,
843 Developments in sedimentology: Elsevier, 183-202.
- 844
- 845

846 **Figures**



847

848

Figure 1: General map of the study area. (A) map from GeoMapApp

849

(<http://www.geomapapp.org>) indicating the main deep water masses interacting with the

850

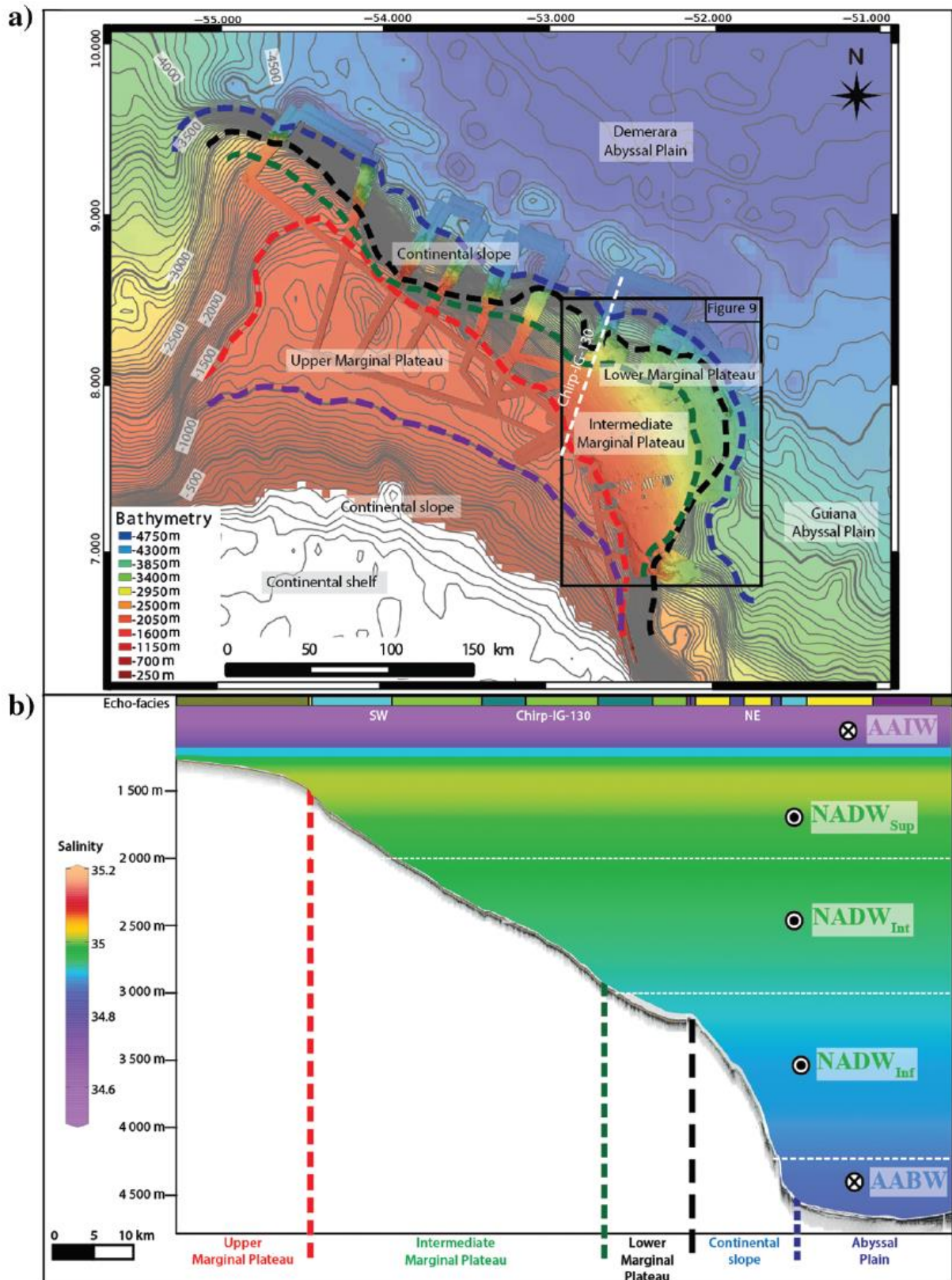
Demerara seafloor; (B) bathymetric map with position of sub-bottom profiles

851

(GUYAPLAC, IGUANES, DRADEM, MARGATS), IGUANES sedimentary cores and

852

the position of the mooring.



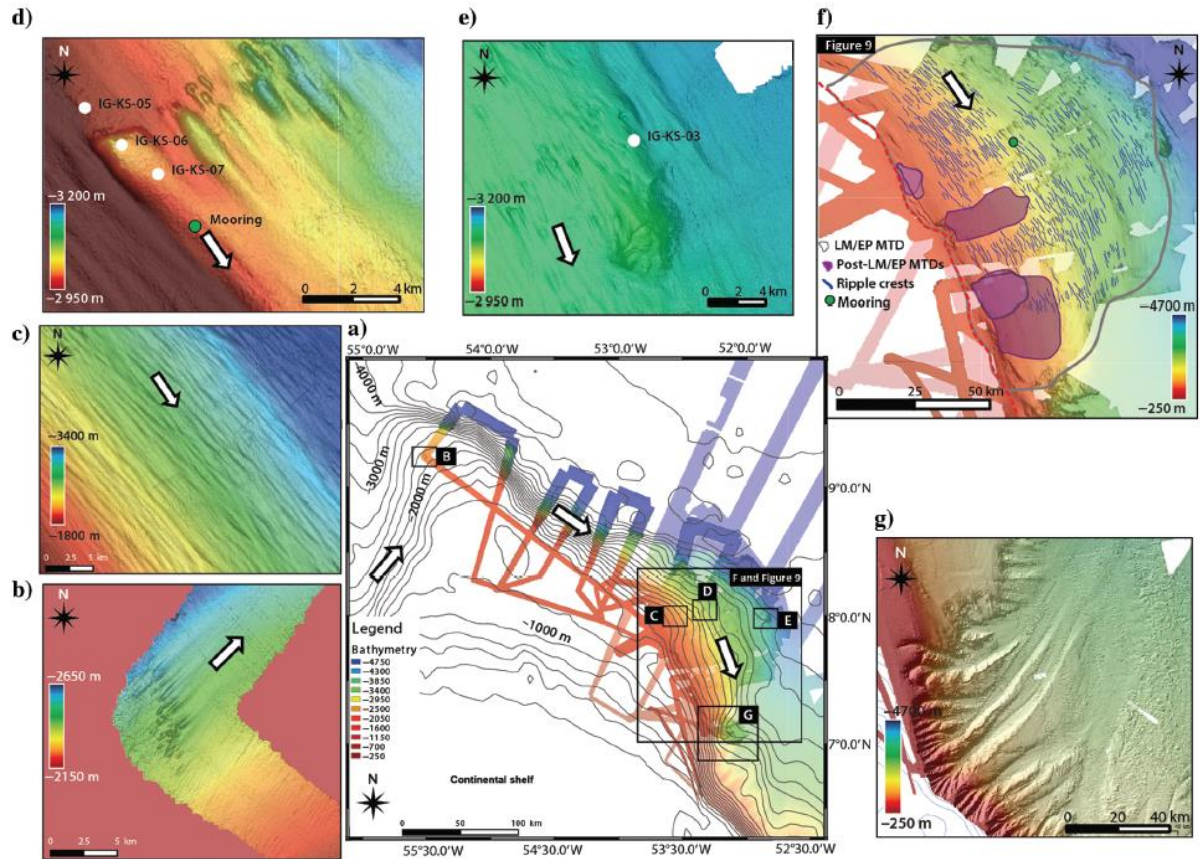
853

854

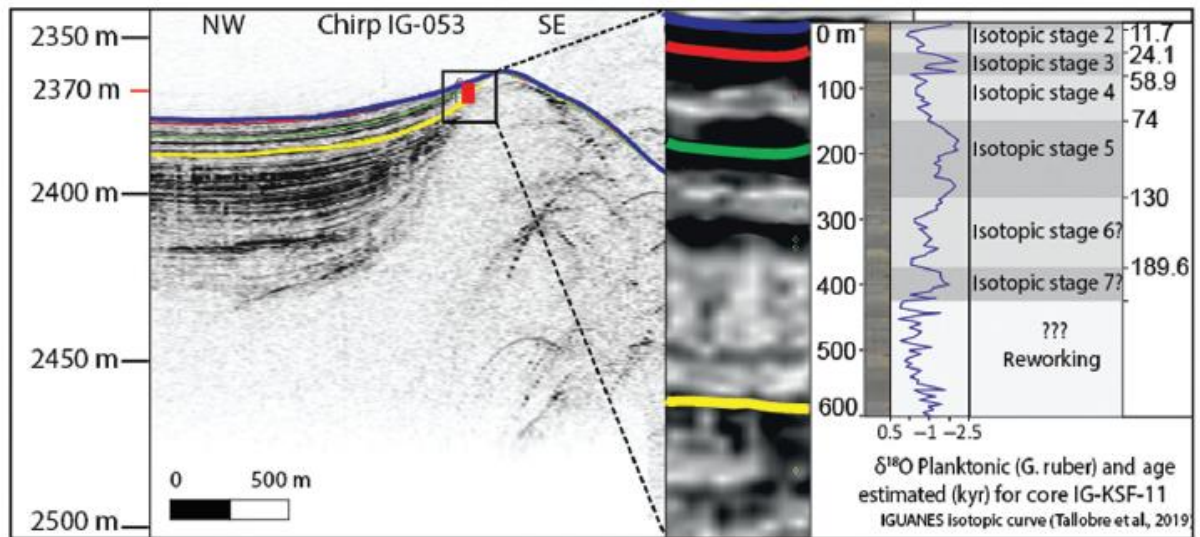
855

Figure 2: (A) Color bathymetric map with 50 m iso-contours spacing; (B) Sub-bottom profile (white line on A) of the Demerara marginal plateau with identification of

856 **the upper plateau, the headscarp slope failure, the intermediate plateau, the lower**
857 **plateau, the continental slope and the position of the water masses, water mass salinity**
858 **values projected from A20 WOCE hydrographic section (Koltermann et al., 2011).**



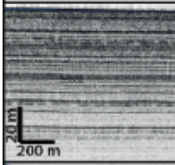
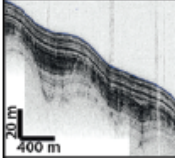
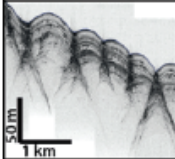
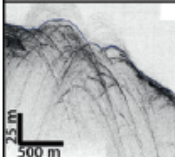
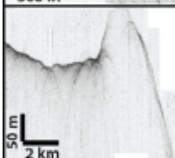
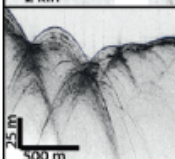
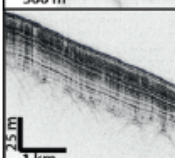
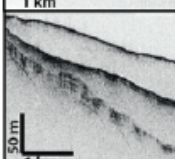
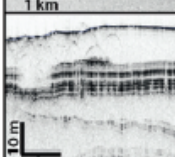
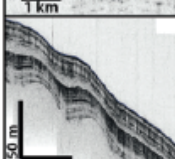
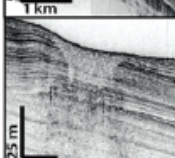
859
860 **Figure 3 : Color bathymetric maps to illustrate the features present on the seafloor.**
861 **(A) bathymetric map with iso-contours spaced 200 m apart; (B) focus on elongated scours**
862 **with comet tails on the west edge of the Demerara marginal plateau oriented N 45°;**
863 **(C) focus on longitudinal waves parallel to the isobaths; (D) focus on the biggest elongated**
864 **scours (4500 m long, 1800 m wide and 49 m of depth) oriented N 128° as the mean**
865 **direction of the NADW measured by the mooring (Tallobre et al., 2016); (E) zoom on the**
866 **topographic mount located on the continental slope; (F) bathymetric map of the eastern**
867 **part of the Demerara marginal plateau with cartography of the MTDs (from Pattier et**
868 **al., (2013)) and crests of the longitudinal waves (modified from Tallobre et al., (2016));**
869 **(G) focus on the south-east corner with the presences of some canyon.**



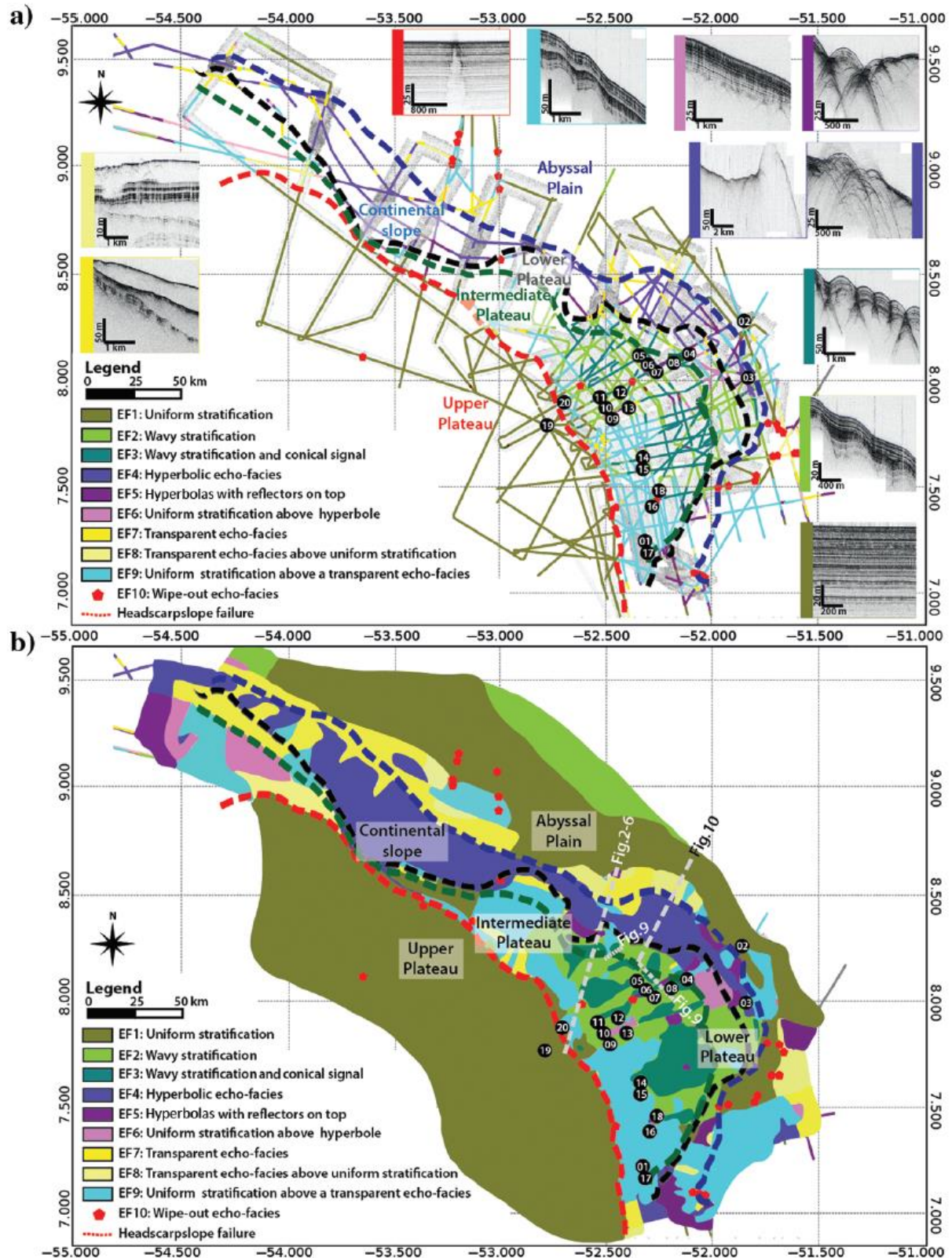
870

871 **Figure 4 : Calibration of sub-bottom profiles by cores and stratigraphy (stratigraphy**

872 **obtained by IGUANES isotopic curve from Tallobre et al., (2019)).**

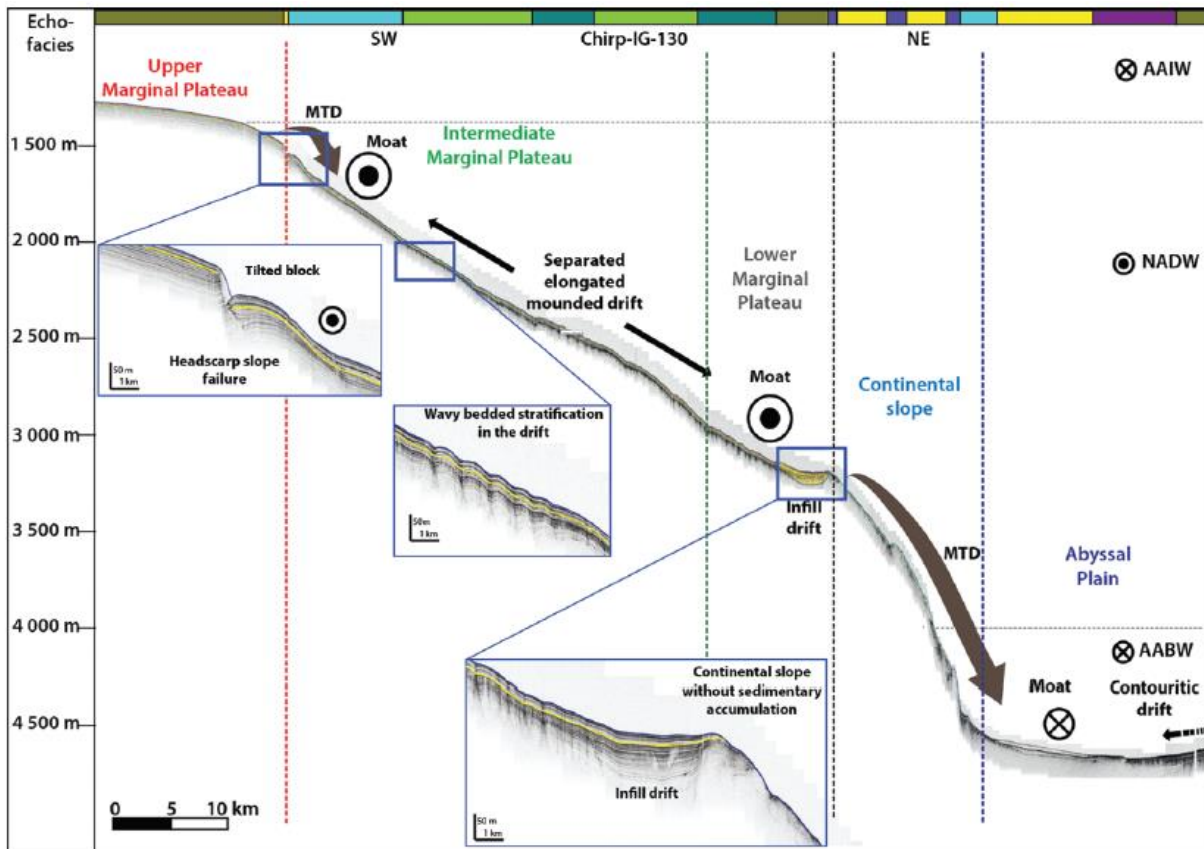
Echo-facies	Designation	Associated sediment types (core data) and stratigraphy	Deposit type
	EF-1 Bedded echo-facies	Pleistocene-Holocene Homogeneous silt and clay muds IG-KS-02 IG-KS-19	Hemipelagic sedimentation ; Turbidite?
	EF-2 Wavy bedded echo-facies	Pleistocene-Holocene Silty sandy sediments with reworked foraminifera and glaucony IG-KS-05 IG-KS-07 IG-KS-14 IG-KS-11 IG-KS-12	Contourite with sedimentary ridges ; Possible hemipelagic component
	EF-3 Wavy stratification and conical signal echo-facies	Pleistocene-Holocene Silty sandy sediments with reworked foraminifera and glaucony IG-KS-08	- Contourite with sedimentary ridges - Conical signal due to diffraction hyperbolae at junction of two ridges, or diffraction hyperbolae linked to a more diffracting sedimentary structure
	EF-4 Hyperbolic echo-facies	Oligocene-Miocene Structureless low content water carbonates IG-KS-03 IG-KS-10 IG-KS-13 IG-KS-16	Slope artifact due to structureless sediments in mass transport deposit ; Indurated sedimentary high
	EF-4 Hyperbolic echo-facies		
	EF-5 Hyperbolae with reflectors on top echo-facies	Structureless carbonates covered by high water content gray-greenish muds IG-KS-04 IG-KS-06	Hemipelagite and contourite covering structureless sediments in mass transport deposit or an indurated sedimentary high
	EF-6 Uniform stratification above hyperbolae echo-facies	Pleistocene-Holocene Silty sandy sediments with reworked foraminifera and glaucony Buried hyperbolae not reached by cores IG-KS-09	Hemipelagite and contourite covering structureless sediments in mass transport deposit
	EF-7 Transparent echo-facies	Not sampled	Structureless sediments in mass transport deposit
	EF-8 Transparent echo-facies above uniform stratification	Not sampled	Structureless sediments in mass transport deposit which cover and eroded the hemipelagite or contourite
	EF-9 Uniform stratification above a transparent echo-facies	Pleistocene-Holocene Silty sandy sediments with reworked foraminifera and glaucony ? Transparent body not reached by cores IG-KS-01 IG-KS-15 IG-KS-17 IG-KS-18 IG-KS-20	Hemipelagite and contourite covering structureless sediments in mass transport deposit
	EF-10 Wipe-out echo-facies	Not sampled	Perturbed acoustic signals, vertical plume associated to fluid circulation (gas or water) in sediment column

874 **Figure 5: Echo-facies classification, interpretation in term of sedimentary types,**
875 **processes and stratigraphy (from Tallobre et al., 2016; Tallobre 2017; and Tallobre et al.,**
876 **2019), illustrated with typical sub-bottom profile sections. When echo-types could be**
877 **calibrated by core data they are labelled “IG-KS” for IGUANES-Kullenberg with a**
878 **number from 1 to 20. All cores are localized in Figure 6 using these labels.**



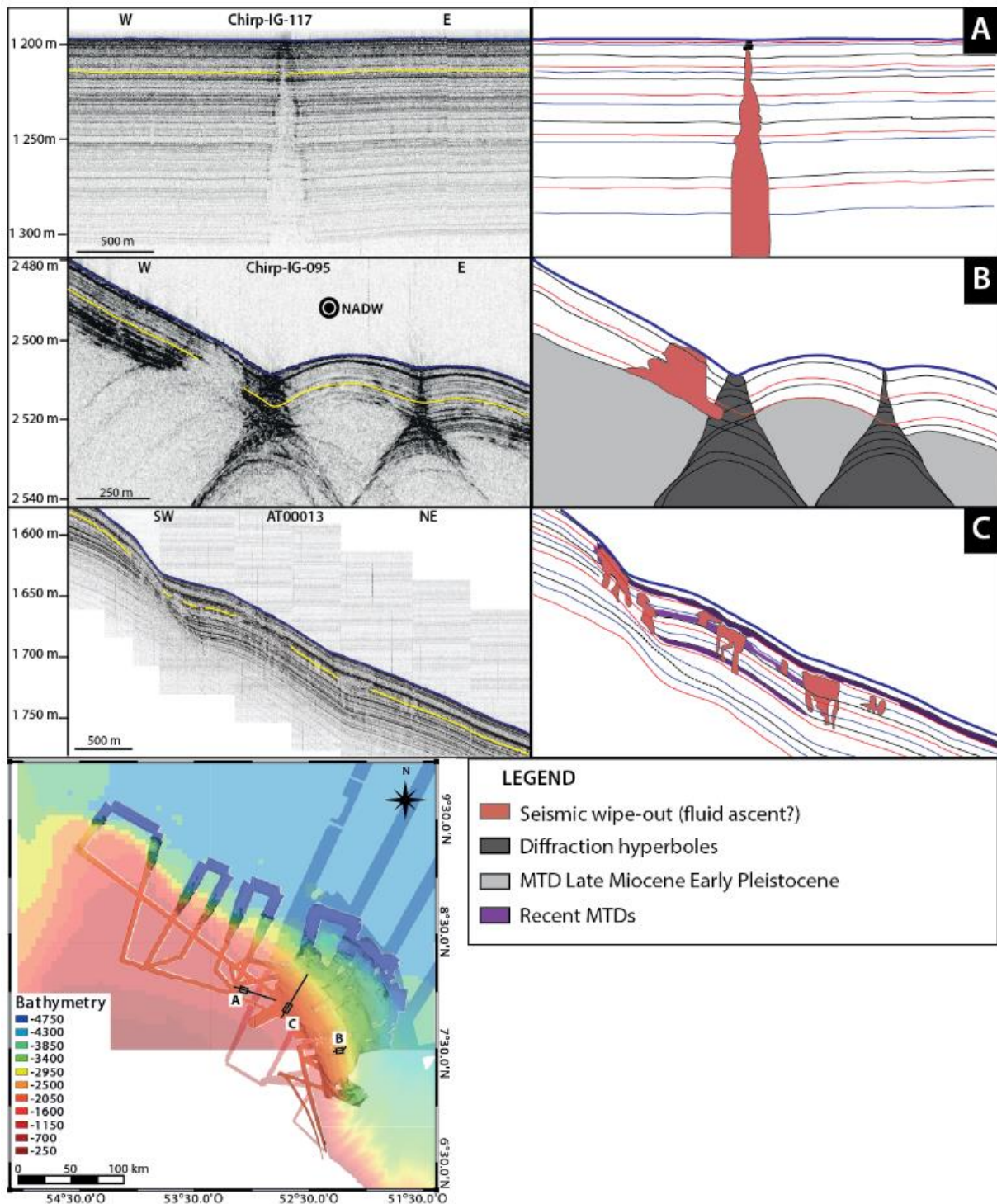
879

880 **Figure 6: Echo-facies map of the Demerara marginal plateau and position of**
 881 **sedimentary cores. (A) map with echo-facies classification and (B) interpolated map of**
 882 **echo-facies distribution and position of sub-bottom profiles used in this study.**



883

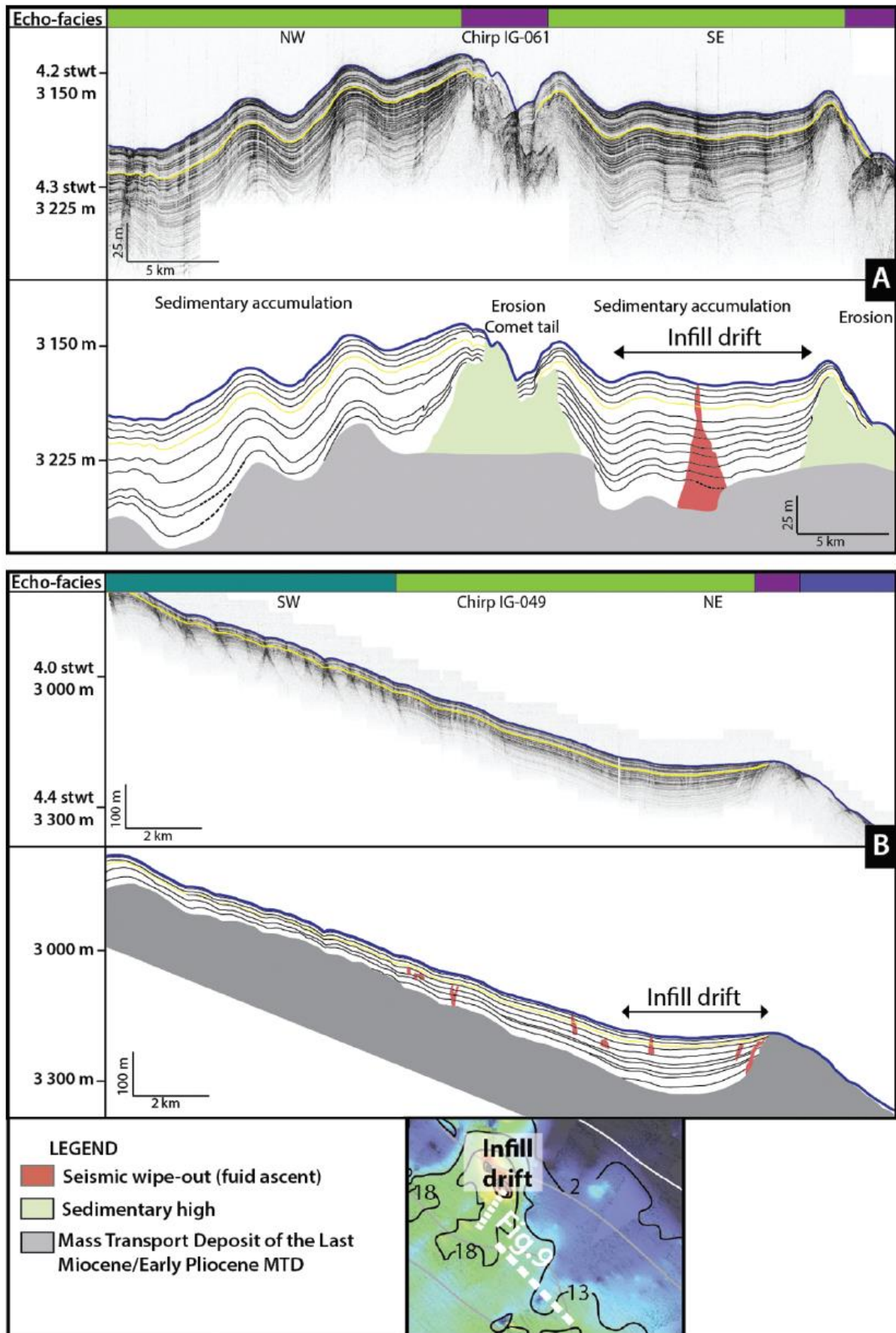
884 **Figure 7: Sub-bottom profile illustrating the main sedimentary processes (MTD,**
885 **contouritic moat, contouritic drifts) as a function of the physiographic domains on the**
886 **Demerara marginal plateau. Location of the SBP line in Figure 6, echo-facies colour codes**
887 **is the same as in figure 5. Note the stratigraphic location of the yellow reflector (see Figure**
888 **4).**



889

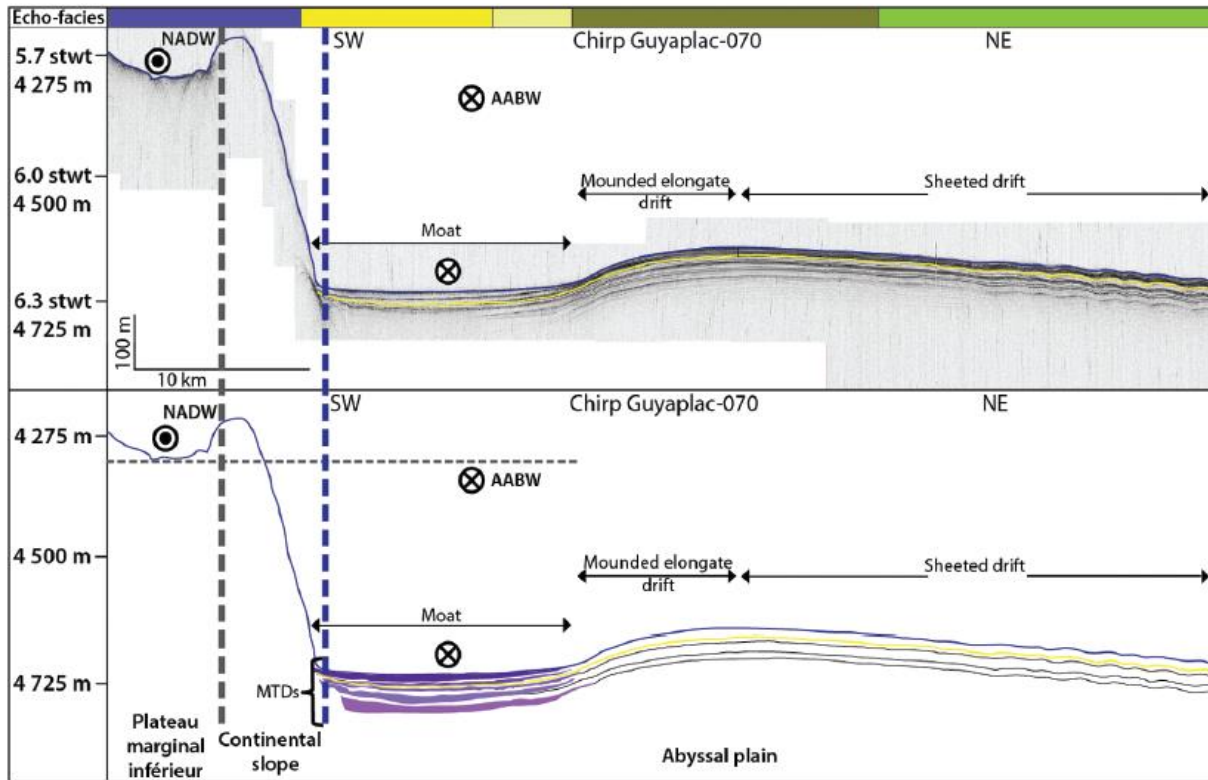
890 **Figure 8: Sub-bottom profiles illustrating the wipe-out echo-facies characterized by**
 891 **perturbed acoustic signals which can be associated to fluid circulation in the sedimentary**
 892 **column. In yellow, the deepest reflector reached by sedimentary cores. Note the**
 893 **stratigraphic location of the yellow reflector (see Figure 4).**

894

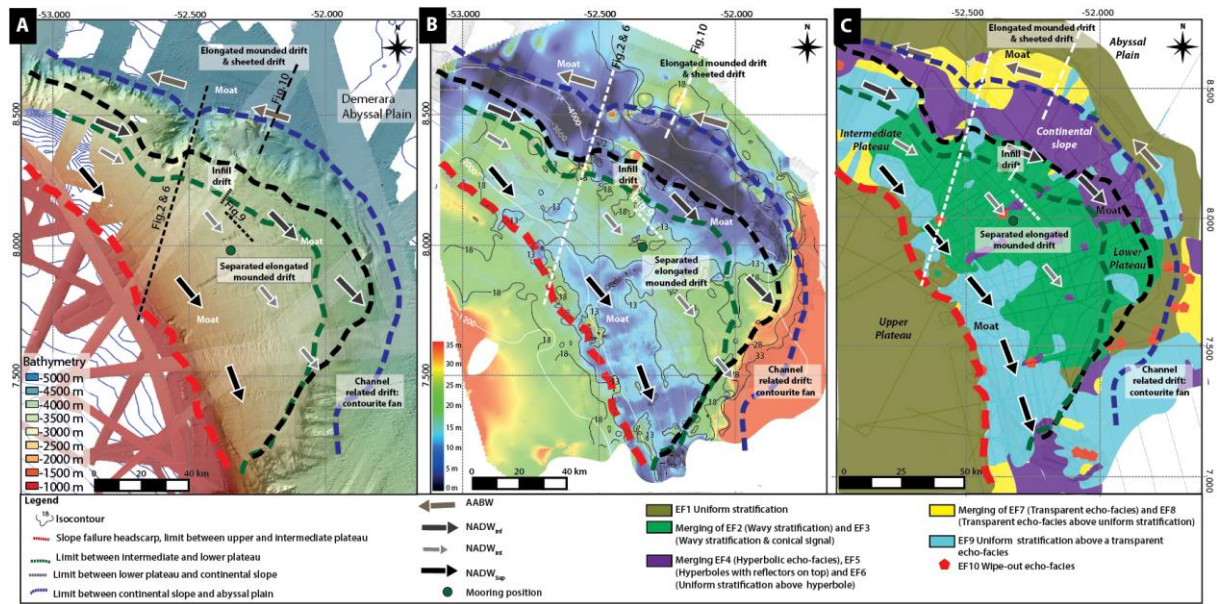


895

896 **Figure 9: Illustrations of the infill drift locally present on the lower marginal plateau.**
897 **Echo-facies color code same as in figure 5. Note the stratigraphic location of the yellow**
898 **reflector (see Figure 4).**



899
900 **Figure 10: Sub-bottom profile illustrating the sedimentary processes present on the**
901 **continental slope of the Demerara plateau and on the abyssal plain, where a contourite**
902 **channel is clearly expressed, it passes laterally to a mounded elongate and then a sheeted**
903 **drift. Location of the SBP line in Figure 2A. Echo-facies color code same as in figure 5.**
904 **Note the stratigraphic location of the yellow reflector (see Figure 4).**



905

906

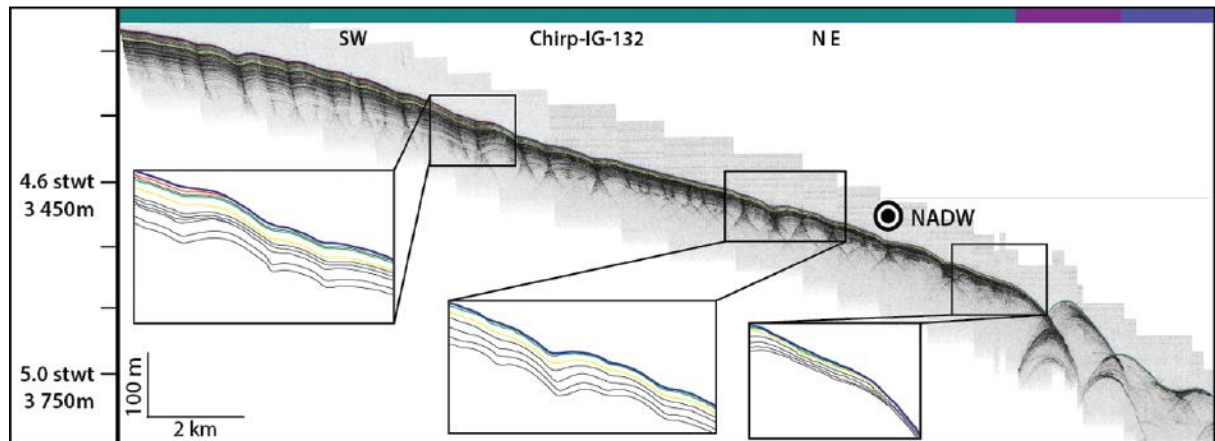
Figure 11: Synthesis of the sedimentary processes on the eastern part of the Demerara plateau with (A) bathymetric map; (B) isopach map of sedimentary deposits calculated between the seafloor and the yellow horizon (visible on the SBP) which is the deepest horizon reached by coring (modified and completed with new data from Tallobre et al, 2016); (C) the up to date echo-facies map presented in this study.

907

908

909

910



911

912

Figure 12: Sub-bottom profile showing the lower marginal plateau. Location of the SBP line in Figure 2A. Echo-facies color code same as in figure 5.

913